Department of High-Tech Engineering

An origami inspired spherical transformable metamaterial based on symmetry groups

I.R. Nuijts

Report no	:
Student number	: 4298780
Daily supervisor	: F.G.J. Broeren Msc.
Professor	: Prof. dr. ir. J.L. Herder
Master	: Mechanical Engineering
Specialisation	: Biomechanical Design
Track	: Bio-Inspired Technology
Type of report	: Master Thesis
Date	: June 2019

TU Delft

An origami inspired spherical transformable meta-material based on symmetry groups

By

I.R. Nuijts

in partial fulfilment of the requirements for the degree of

Master of Science
in Mechanical Engineering

at the Delft University of Technology,
to be defended publicly on Wednesday June 29, 2019 at 10:00 AM.

Supervisor:	Prof. dr. ir. J.L. Herder	TU Delft
Thesis committee:	Dr. ir. V. van der Wijk,	TU Delft
	Dr. ir. G. Smit,	TU Delft
	F.G.J. Broeren Msc	TU Delft

This thesis is confidential and cannot be made public until December 31, 2019.

An electronic version of this thesis is available at http://repository.tudelft.nl/.

Preface

This thesis is the final product of the master Biomechanical Design from the faculty Mechanical, Maritime and Materials Engineering at the Delft University of Technology. I started the bachelor study of Mechanical Engineering in September of 2013. After finishing the bachelor I started with the Mechanical Engineering master, specialisation Biomechanical Design and track Bio-Inspired Technologies. The masters theses from this specialisation were not in line with my interests and so I arrived at High-Tech Engineering where I met Freek Broeren, who was at the time investigating more interesting concepts.

I would like to thank Freek Broeren for his weekly feedback and support for almost a year. I would also like to thank Volkert van der Wijk for his constructive feedback and guiding and the supporting staff at the High-Tech Engineering workspace for helping during the fabrication process. Lastly I would like to thank my friends and family for supporting and helping during my whole academic career at TU Delft.

I.R. Nuijts
Delft, June 2019

Contents

1

Introduction

In this thesis, a mechanical metamaterial will be developed, which is based on spherical symmetry groups and inspired by origami. Metamaterials are materials with counter-intuitive properties which are engineered and thus not found in nature. These man-made metamaterials open up a variety of innovations due to having properties which were never seen before, such as a negative index of refraction, negative Poisson's ratio (auxetic metamaterials) or having vanishing sheer stress [1]–[3]. These properties ensured that metamaterials have found their application in fields such as electrical engineering, electromagnetics, classical optics, material sciences and many others [3]–[5]. But also in sports as, for example, impact protector devices [6] and in surgery as auxetic blood vessels, which increase in wall thickness as a response to a pulse of blood flowing through it [7].

If the metamaterial has mechanical properties which are counter-intuitive, it is categorized as a mechanical metamaterial, which is a specific type of metamaterials. Part of these materials are the auxetic metamaterials. When stretched, auxetic metamaterials expand in the direction perpendicular to the applied load [8]. Mechanical metamaterials, and more precisely: auxetic metamaterials, will be discussed in more detail in the literature survey.

Most metamaterials have a periodic structure; they consist of a unit cell, which is repeated periodically throughout the structure. These metamaterials are usually arranged in repeating patterns to form a structure. This is done by discrete translations along the lattice vectors of different Bravais Lattices [9], [10]. The objective of this study is to identify the design possibilities of spherical symmetries as opposed to the standard symmetries used in current metamaterial studies. There have been multiple studies on spherical symmetries [11], [12], however, to the authors knowledge, they remain unseen for engineering purposes. If the possibilities of developing structures based spherical symmetries are explored, it could possibly open up a whole different branch of structures. For example for projecting auxetic structures on curved surfaces.

Origami is used as a source of inspiration due to the fact that ideas can quickly be modelled with a piece of paper in order to test different possibilities and to grow intuition for the subject. If a model works properly when made out of paper, it can be used as a foundation for more complex structures. From an engineering point of view, origami functions as rigid body mechanics. Furthermore, a very well-known origami fold, the Miura-Ori fold [13], [14], has its functions as an auxetic structure for engineering purposes [15].

Thesis outline

This thesis is structured as followed: First, a literature survey on metamaterials and auxetics is presented. From this survey the current research gap is stated. Secondly, a paper concerning spherical symmetries is presented. In this paper an origami inspired metamaterial based on a spherical symmetry-group is modelled, fabricated and tested. Lastly a general discussion and conclusion is presented.

2

Classifications of auxetic metamaterials and their periodicities

Classifications of auxetic metamaterials and their periodicities

Literature review by Ivar R. Nuijts
TU Delft, Department of Mechanical Engineering, Maritime Engineering and Materials Engineering (3mE)

Abstract - Metamaterials are materials engineered to have certain properties not normally found in nature. Mechanical metamaterials are a branch of metamaterials with counterintuitive mechanical properties, such as a negative Poisson's ratio. These types of materials are categorized as auxetic metamaterials, or specifically, metamaterials with a Poisson's ratio of -1 are called dilational metamaterials. Auxetic materials have been developed both for two-dimensional planes as well as three-dimensional structures by constructing a unit cell and then repeating it periodically to form the whole structure. Different types of origami folds exhibit auxetic behaviour as well when folded. This survey discusses a few types of auxetic structures, both two-dimensional and three-dimensional. The survey concludes with stating the current research gap of the auxetic metamaterials and proposes origami as a possibility for future developed auxetic structures.

1. Introduction

Metamaterials have rose in popularity due to their counterintuitive properties leading to many interesting possibilities surrounding them [1]–[3]. The advances in computational tools, theoretical advances and increases in experimental techniques [4], make the development of metamaterials possible on a nano- and microscale.

Metamaterials are materials not found in nature but engineered by combining different materials to have the desired properties [1], [5]. All materials found in nature, such as glass and diamond, have positive values for, for instance, electrical permittivity, magnetic permeability and index of refraction. However, for metamaterials it is possible that these parameters are negative [1]. Due to these counterintuitive properties, metamaterials have found their place in electrical engineering, electromagnetics, optics and many other fields [6].

In this survey different types of metamaterials will be briefly discussed and quickly the focus will lie on auxetic metamaterials. Auxetic materials are defined as materials that upon stretching, become thicker perpendicular to the applied force. Different types of auxetic materials will be discussed, together with origami folds that also exhibit auxetic behaviour. This will be used to formulate the current research gap and possibilities for further research that use different types of symmetry groups.

2. Mechanical Metamaterials

Research in metamaterials started in the field of optics [2], but soon branched out to other fields such as acoustics and mechanics. Mechanical metamaterials

are metamaterials engineered with specific mechanical properties that are not found in nature, for example having a negative Poisson's ratio (ν) [7]–[10] or having vanishing shear stresses [11]–[13].

As a starting point, the focus lies on metamaterials with interesting properties regarding Poisson's ratio, i.e. values that lie on the edge of the possible range for the Poisson's ratio in classical materials. Poisson's ratio is defined as the amount of transversal expansion divided by the amount of axial compression, for small deformations of the material. For three-dimensional isotropic materials the Poisson's ratio is related to the bulk modulus, B, and shear modulus, G, by the following formula [5]:

$$\frac{B}{G} = \frac{\nu + 1}{3\left(\frac{1}{2} - \nu\right)}$$

To ensure that the material is thermodynamically stable, B and G are assumed positive. This leads to a range of ν of (-1, 0.5). Zadpoor [5] discusses metamaterials that lie on the edge of the spectrum of the Poisson's ratio for isotropic materials. Namely 'penta-mode metamaterials' with a ratio of 0.5 and the above mentioned dilational metamaterials with a ratio of -1. Zadpoor uses the term 'Extremal materials' to describe these materials, since they exhibit extreme behaviour with respect to ν.

Penta-mode metamaterials are compliant in five of the six principal directions, as the name implies [5]. These materials have an extremely high bulk modulus compared to their shear modulus and as a result heavily resist volume changes but are very compliant to shear deformations [12], [14], making the materials 'flow away' if being subjected to shear forces. This behaviour has earned them the name of 'meta-fluids' [12]. Due to the specific properties of penta-mode metamaterials, they are well suited for certain applications, such as steering elastodynamic waves in specific directions to achieve the equivalent of optical cloaking for acoustic waves [12] or a gel that can be easily deformed in any given direction but resists volume changes [15].

Dilational metamaterials, in contrast to penta-mode metamaterials, have an extremely high shear modulus compared to the bulk modulus. This means that these materials easily change volume but remain the exact same shape. Which is the same as stating that the Poisson's ratio is equal to -1. An intuitive example to clarify this behaviour is given by Bückmann et al. [16] where he uses the Statue of Liberty as an example. If one would exert a force anywhere on the statue and in any direction, the statue would easily change volume, but would remain the exact same shape.

3. Auxetic metamaterials

Auxetic materials have been extensively studied before [17]. A few of these studies will be reflected on in this chapter. Auxetic materials can be divided between naturally occurring auxetic materials and man-made auxetic materials.

3.1 Natural auxetic materials

Auxetic materials, despite having a counterintuitive behaviour towards external forces, do appear naturally. For example on a molecular level in naturally occurring single-crystal materials such as arsenic and cadmium [18]. Naturally occurring auxetic

biomaterials are also existent, examples include cow teat skin and cat skin [18].

A more well-known field are those of the auxetic foams[10], [19]. The first one to study auxetic foams is Robert lakes in '*Foam Structures with a Negative Poisson's ratio'* [10] in 1987. Since these foams are man-made, they could be regarded as an in-between form of natural and engineered materials. For auxetic foams, it has been determined that the value of the Poisson's ratio varies with the strain of the material, reaching towards the lower boundary of -1 for isotropic materials. For polymeric and metallic isotropic materials, values of ν of -0.7 and -0.8 respectively have been reported [18]. Auxetic foams have found an application in sports, mainly for protection as impact protectors in pads, gloves and helmets [19].

3.2 Man-made auxetic metamaterials

Two-dimensional auxetic metamaterials have received a lot of attention in design studies [20]. These studies often take a small square, or rectangle, referred to as a unit cell [16], [21], [22] that behaves in an auxetic manner and repeat them along a plane. Because the plane is structured as a unit cell repeated in two directions and the deformations in a unit cell are assumed to be periodic, if the unit cell has ν=-1, the whole plane will as well. The assumption that the deformations are periodic is not always in compliance with reality since it does not have to correspond with the actual kinematics of the structure, see [23] for an in-depth explanation. This method is still the best course of action for creating theoretical models of entire auxetic structures, without it being excessively time-consuming.

Studies on auxetic behaviour have been done with a wide range of different types of unit cells. These unit cells are, for example, composed of isotropic elastic materials [16], composite materials [9] or, for prescribing the motion kinematically, by means of rigid links an hinges [20] or a rotating squares model [21]. Some of these studies aim to invent new dilational materials [24], while some focus only on auxetic behaviour.

Auxetic structures that have the deformation of their representative unit dominated by a rotational motion are called 'chiral structures' [8], [17], [25]. This concept has also been implemented as a periodic two-dimensional structure. For a chiral structure, the unit cell has to be chiral and the global structure has to have the same chirality [8]. This means that the unit cell is build up by rotational symmetry only, see fig. 1.

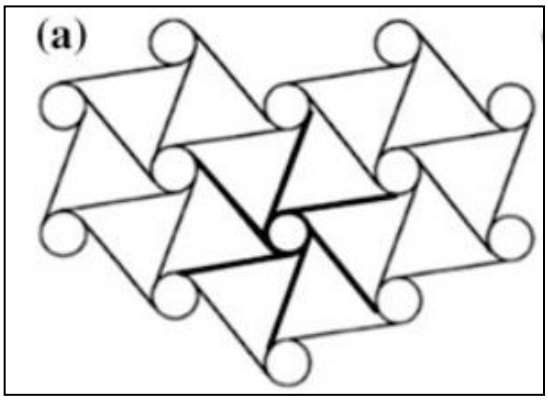

Figure 1. Typical structure with mono chiralty, from [8].

If the unit cell exhibits auxetic rotational behaviour, but the unit cell has a mirror symmetry, rather than a rotational symmetry, the structure is known as *non-chiral*, or *anti-chiral* [2], see fig. 2.

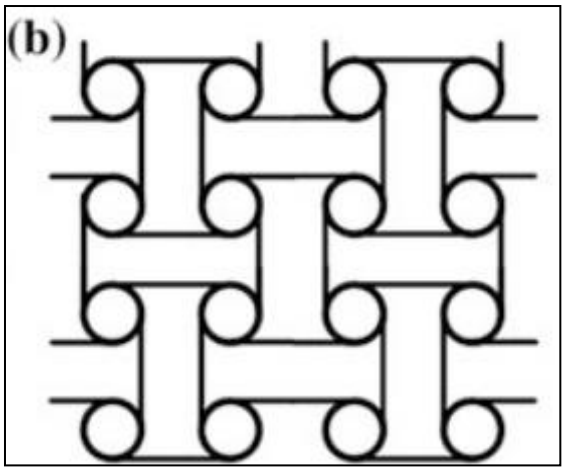

Figure 2. Anti-chiral structure. The unit cells alternate between each other by turning clockwise and counter clockwise, from [8].

These structures are often considered non-periodic, however these structures are build up by different symmetries, i.e. mirror symmetries. Meaning that anti-chiral structures are, in fact, periodic, only with a larger unit cell. This raises the question what other unit cells can be developed by considering different types of symmetries to create periodic structures.

Three-dimensional structures with auxetic behaviour are a more challenging field of study, often relying on the same principles as its two-dimensional variant, having a periodic framework made up of a three-dimensional unit cell [15], [16], [26]–[28]. Borcea and Streinu [28] provide mathematical proof for necessary geometric conditions of such a cubic unit cell in order to build an auxetic periodic framework. They do so by representing their structure as a periodic bar-and-joint framework then use this principle to construct a variety of three-dimensional auxetic periodic mechanisms and discuss the ideas involved in their design.

A different approach is presented by Bückmann et al. [16]. Here a three-dimensional cubic unit cell classified as non-chiral is used. Bückmann begins in his introduction by stating that for some materials and structures, perfect dilational behaviour is only theoretically possible, since it relies on perfectly rigid links and ideal hinges. Which are links that will never bend and hinges without volume or contact area. All of these are not possible in an actual model. Bückmann modelled a cubic unit cell in COMSOL, see fig. 3, and also fabricated a real unit cell with the use of three-dimensional printing technologies, which is shown in fig. 4.

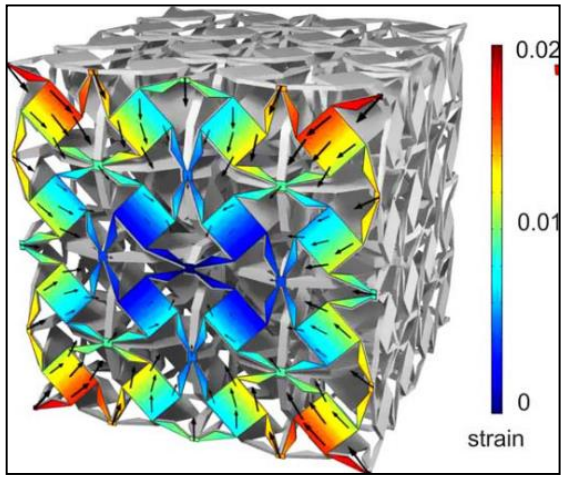

Figure 3. A 2x2x2 unit cell modelled in COMSOL with resulting in-plane strain for axial strain depicted, from [16].

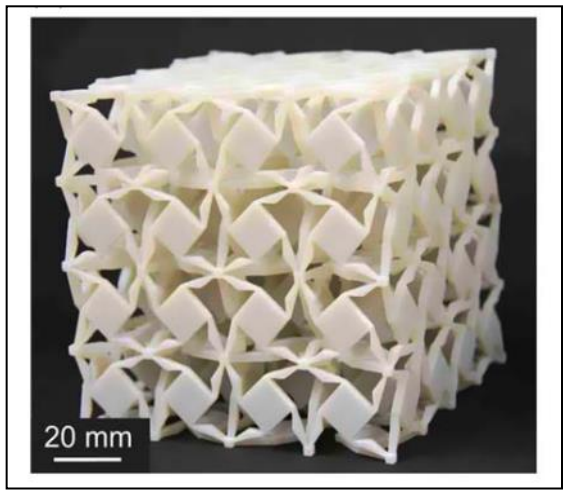

Figure 4. A 3D printed unit cell, from [16].

Bückmann calculates the phonon band structures to determine all the modes of the elastic meta-material. His blueprint contains small internal connections, *d/a*, to mimic the abovementioned 'ideal hinges'. Bückmann made a graph of the phonon band structures for two different values of d/a. An important discovery made by Bückmann in this paper is the relation of the Poisson's ratio versus the size of the internal connections. See fig. 5.

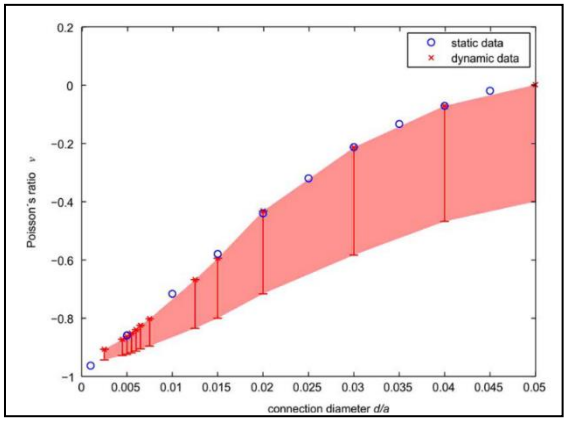

Figure 5. The minimum and maximum effective metamaterial Poisson's ratio, from [16].

This conclusion provides an important point of attention for future developed dilational models, namely that internal connections should as be as small as possible if one wishes to fabricate dilational metamaterials.

3.3 Auxetic origami folds

Origami, the Japanese art of paperfolding, has found its applications in engineering. Using a broader definition for origami: creating three-dimensional structures from folding two-dimensional sheets, not necessarily paper; made it useful in different fields, such as space exploration, as a foldable telescope lens, and automotive safety, such as airbags [29]. In engineering, origami has been considered as rigid body mechanisms, consisting of rigid plates connected by in-plane hinges [30].

Origami has structures with auxetic behaviour as well. Most notably the Miura Ori fold, invented by Koryo Miura. The Miura Ori fold is well known for having a negative Poisson's ratio [29], [31], [32] and for its application in astronautical engineering [33]. For harnessing solar energy, rockets would orbit around the sun with solar panels. To do so, the solar panels would need to fold up as much as possible in order to stack them in the rocket for launch. For minimizing the area of the panels the Miura-Ori fold was used. The Miura-Ori fold is exceptionally suitable for this purpose, not only for it has a negative ν, but also because it is flat-foldable. Geometrically, this means that the fold lines have a range of [-180°, 180°].

In *'Geometry of Miura-folded metamaterials'* [32] by Schenk and Guest they research what exactly are the factors of the Miura Ori pattern that influence the Poisson's ratio. They do so by taking a unit cell of the Miura fold and parameterizing every angle and dimension of it. This unit cell consists of '*three-to-one four-vertex folds'* with every face being a parallelogram. A three-to-one fold is a vertex intersection of four folding lines with one of the four folds being folded in the opposite direction with respect to the other three. Using the definition that the Poisson's ratio is defined as the negative ratio between the transversal strain and the axial strain, they determined what dimensions of the unit cell have an influence on the Poisson's ratio. They found that only two adjustable angles define the ratio of the fold. By fixing one angle for specific values they plotted the other angle versus the Poisson's ratio, see fig. 6.

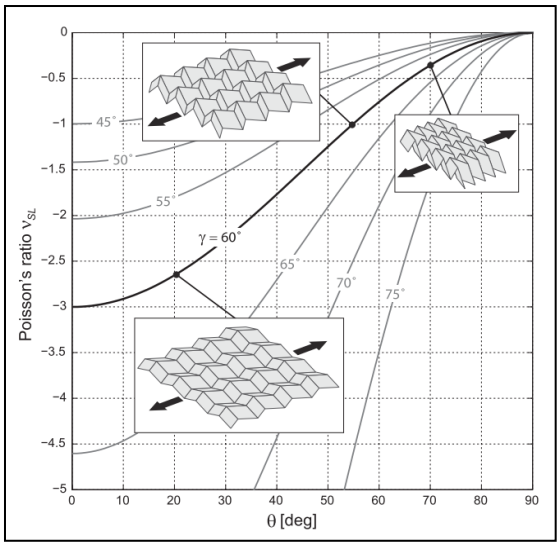

Figure 6. The in-plane expansion coefficent of a Miura-ori sheet, from [32].

From the figure it is clear the Poisson's ratio of the Miura-Ori fold can never be constant, and therefore the Miura-Ori fold is not a dilational fold pattern. However, origami poses a lot of possibilities for designing other auxetic structures, which may be of use when designing new structures.

Not only the Miura-Ori fold exhibits auxetic behaviour. In general, all zig-zag based patterns in origami behave in such a manner. Eidini and Paulino [31] have done an extensive study on zigzag based flat folded sheets. In this paper they start off with the standard Miura-Ori fold and alter it slightly using kirigami, the concept of folding and cutting paper, to create a new structure. This process is seen in fig. 7.

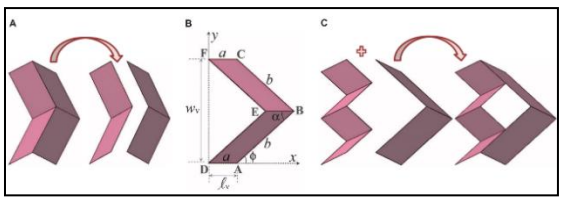

Figure 7. Transformation of a Miura-ori unit cell to a Basic unit cell with hole, from [31].

The unit cell of this new structure has a hole in it and therefore Eidini and Paulino named it Basic unit Cell with Hole (BCH_n). This unit cell includes two large and 2n small parallelogram rigid panels joined via fold lines. Eidini and Paulino used mostly n=2 in their paper.

Eidini did another study on zigzag-based folded elements [34]. In this paper a new zigzag based folded sheet is presented, again based on the Miura-Ori fold and with the use of kirigami. The unit cell of this structure is called Zigzag unit Cell with Hole (ZCH). The methods and results are similar to the previous paper with only the base unit cell being different, resulting in that Poisson's ratio's lower than -4 have been reached. See fig. 8 for the construction of this unit cell and see fig. 2 in their paper for multiple configuration based on the same principle.

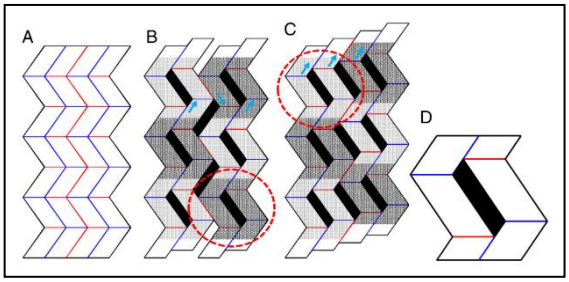

Figure 8. Transformation of a Miura-ori sheet to a zigzag unit sheet with hole, from [34].

Another adaptation of the Miura fold is in the form of a cylinder and is named the Tachi-Miura polyhedron and exhibits bellowslike folding [35], similar to how an accordion moves in and out. In contrast to two-dimensional origami structures, this structure changes it volume upon folding and is also flat foldable. The Tachi-Miura polyhedron has the added benefit of being rigidly foldable, meaning that its Poisson's ratio can be expressed purely geometrically. In [35] Yasuda and Yang do so by examining the kinematics of this structure in order to show the adjustable characteristics of the Poisson's ratio. They verify the auxetic behaviour of the Tachi-Miura

polyhedron in bilateral direction in an analytical and experimental manner. Based on the plots in fig. 2 in [35] it shows that a negative Poisson's ratio is possible for certain angles of inner fold lines and for specific folding ratio's. However, an isotropic negative Poisson's ratio seems impossible.

From the examples above, it becomes clear that the majority of research on auxetic origami is based on the Miura-Ori. However, to the authors knowledge, these studies have not resulted in a structure with a constant Poisson's ratio and therefore dilational behaviour has remained out of reach. This raises the question what other origami folds are possible that exhibit auxetic behaviour, whilst also have a constant Poisson's ratio.

4. Discussion

When reviewing the state-of-the-art of auxetic two-dimensional and three-dimensional models, it becomes clear that they all follow a similar pattern; an auxetic unit cell is developed, sometimes based on chirality or molecular structures, and repeated along a plane. For three-dimensional structures the method is similar; a parallelepipedal unit cell is repeated through the volume. Because the three-dimensional unit cells are repeated periodically to form the whole structure, the structure can be classified as one of the fourteen three-dimensional Bravais lattices [13], [27]. A Bravais lattice is a set of discrete points generated by discrete translations, meaning Bravais lattices can tile all types of rectangular prisms correctly, but cannot tile a spherical surfaces. This raises the question if it is possible to design a unit cell which does not have the conventional shapes, i.e. rectangular or cubic, and repeating them not following these Bravais lattices, but rather using different types of symmetry groups. If this would be implemented, it could benefit design studies that want to project auxetics fittingly on curved surfaces, unlike what is done in [36], where the auxetic sheets are projected flat on a dome, disregarding the curvature.

An idea would be to design a dilational sphere by means of spherical symmetries. There have been studies researching spherical symmetries [37] that could act useful in finding innovative designs based on different types of symmetries from the standard Bravais lattices. The sphere is chosen as a starting point for its simplistic three-dimensional form.

Origami could pose as a solution for this research question, having a rich background in planar patterns, as well as some of these patterns having negative Poisson's ratio's, such as the Miura-Ori fold. New origami folds may be developed, supporting these new proposed methods. To classify which folds are able to rigidly fold, multiple theories have been proposed, and proven [38]–[40]. Combining what is known about spherical symmetries with the multiple possibilities that lie with origami and the newly arising field of dilational metamaterials, an interesting design question arises: What are the possibilities in designing a dilational sphere based on spherical symmetry groups?

5. Conclusion

Mechanical metamaterials are a new class of engineered materials with properties not found in nature. One type of these materials, the auxetic metamaterials, are especially interesting due to their counter-intuitive reaction to external forces. Namely that

they become thicker perpendicular to the applied force. In this paper, examples of two-dimensional, three-dimensional and origami auxetic structures have been presented. It showed that the construction of these materials follow similar patterns; a unit cell is developed and then repeated periodically following Bravais lattices. Using different types of symmetries, new, non-conventional, auxetic structures could be developed and the rigid body mechanics of origami could prove to be useful.

Bibliography

[1] R. S. Kshetrimayum, “A brief intro to metamaterials,” *IEEE Potentials*, vol. 23, no. 5, pp. 44–46, 2004.

[2] X. Yu, J. Zhou, H. Liang, Z. Jiang, and L. Wu, “Mechanical metamaterials associated with stiffness, rigidity and compressibility: A brief review,” *Prog. Mater. Sci.*, vol. 94, pp. 114–173, May 2018.

[3] M. K. Konakovi´c *et al.*, “Beyond Developable: Computational Design and Fabrication with Auxetic Materials.”

[4] P. M. Reis, H. M. Jaeger, and M. van Hecke, “Designer Matter: A perspective,” *Extrem. Mech. Lett.*, vol. 5, pp. 25–29, 2015.

[5] A. A. Zadpoor, “Mechanical meta-materials,” *Mater. Horizons*, vol. 3, no. 5, pp. 371–381, 2016.

[6] S. Zouhdi, A. Sivola, and A. P. Vinogradov, *Metamaterials and Plasmonics: Fundamentals, Modelling, Applications*. 2008.

[7] L. Rothenburg, A. A. Berlin, and R. J. Bathurst, “Microstructure of isotropic materials with negative Poisson’s ratio,” *Lett. to Nat.*, 1991.

[8] X. Hou and V. V. Silberschmidt, “Metamaterials with Negative Poisson’s Ratio: A Review of Mechanical Properties and Deformation Mechanisms,” in *Mechanics of Advanced Materials*, Springer, Cham, 2015, pp. 155–179.

[9] G. W. Milton, “COMPOSITE MATERIALS WITH POISSON’S RATIOS CLOSE TO-1,” *Mech. Phys. Solids*, vol. 40, no. 5, pp. 1105–1137, 1992.

[10] R. Lakes, “Foam Structures with a Negative Poisson’s ratio,” *Science (80-.).*, vol. 235, pp. 1038–1040, 1987.

[11] M. Kadic, T. Bückmann, N. Stenger, M. Thiel, and M. Wegener, “Elastic measurements on macroscopic three-dimensional pentamode metamaterials,” *Acoust. metafluids J. Acoust. Soc. Am.*, vol. 100, p. 2856, 2012.

[12] M. Kadic, T. Bückmann, N. Stenger, M. Thiel, and M. Wegener, “On the practicability of pentamode mechanical metamaterials,” *Appl. Phys. Lett.*, vol. 100, no. 19, p. 191901, May 2012.

[13] G. F. Méjica and A. D. Lantada, “Comparative study of potential pentamodal metamaterials inspired by Bravais lattices,” *Smart Mater. Struct.*, vol. 22, no. 11, 2013.

[14] R. Schittny, T. Bückmann, M. Kadic, and M. Wegener, “Elastic measurements on macroscopic three-dimensional pentamode metamaterials,” *Cit. Appl. Phys. Lett*, vol. 103, p. 231905, 2013.

[15] G. W. Milton, “Complete characterization of the macroscopic deformations of periodic unimode metamaterials of rigid bars and pivots,” 2012.

[16] T. Bückmann, R. Schittny, M. Thiel, M. Kadic, G. W. Milton,

and M. Wegener, “On three-dimensional dilational elastic metamaterials,” *New J. Phys.*, vol. 16, 2014.
[17] Y. Liu and H. Hu, “A review on auxetic structures and polymeric materials,” *Sci. Res. Essays*, vol. 5, no. 10, pp. 1052–1063, 2010.
[18] K. E. Evans and A. Alderson, “Auxetic materials: Functional materials and structures from lateral thinking!,” *Adv. Mater.*, vol. 12, no. 9, pp. 617–628, 2000.
[19] M. Sanami, N. Ravirala, K. Alderson, and A. Alderson, “ScienceDirect Auxetic materials for sports applications,” *Procedia Eng.*, vol. 72, pp. 453–458, 2014.
[20] L. Cabras and M. Brun, “Auxetic two-dimensional lattices with Poisson ’ s ratio arbitrarily close to − 1,” *Proc. R. Soc. A*, vol. 470, no. October, p. 20140538, 2014.
[21] J. N. Grima and K. E. Evans, “Auxetic behavior from rotating squares,” *J. Mater. Sci. Lett.*, vol. 19, no. 17, pp. 1563–1565, 2000.
[22] X. Yu, J. Zhou, H. Liang, Z. Jiang, and L. Wu, “Mechanical metamaterials associated with stiffness, rigidity and compressibility: A brief review,” *Prog. Mater. Sci.*, vol. 94, pp. 114–173, 2018.
[23] R. G. Hutchinson and N. A. Fleck, “The structural performance of the periodic truss,” *J. Mech. Phys. Solids*, vol. 54, pp. 756–782, 2006.
[24] G. W. Milton, “New examples of three-dimensional dilational materials,” *Phys. Status Solidi Basic Res.*, vol. 252, no. 7, pp. 1426–1430, 2015.
[25] Y. Zárate *et al.*, “Elastic metamaterials for tuning circular polarization of electromagnetic waves,” *Sci. Rep.*, vol. 6, 2016.
[26] J. T. B. Overvelde *et al.*, “A three-dimensional actuated origami-inspired transformable metamaterial with multiple degrees of freedom,” *Nat. Commun.*, 2016.
[27] L. Cabras and M. Brun, “A class of auxetic three-dimensional lattices,” *J. Mech. Phys. Solids*, vol. 91, pp. 56–72, 2016.
[28] C. S. Borcea and I. Streinu, “Auxetics Abounding,” 2018.
[29] C. Lv, D. Krishnaraju, G. Konjevod, H. Yu, and H. Jiang, “Origami based Mechanical Metamaterials,” *Sci. Rep.*, vol. 1, 2014.
[30] T. Tachi, “Simulation of Rigid Origami Self-Foldability View project Simulation of Rigid Origami,” 2009.
[31] M. Eidini and G. H. Paulino, “Unraveling metamaterial properties in zigzag-base folded sheets,” *Mater. Sci.*, no. September, pp. 1–8, 2015.
[32] M. Schenk and S. D. Guest, “Geometry of Miura-folded metamaterials,” *PNAS*, vol. 110, no. 9, pp. 3276–3281, 2013.
[33] Y. Nishiyama, “Miura Folding: Applying Origami to Space Exploration.”
[34] M. Eidini, “Zigzag-base folded sheet cellular mechanical metamaterials,” *Extrem. Mech. Lett.*, vol. 6, pp. 96–102, 2016.
[35] H. Yasuda and J. Yang, “Reentrant Origami-Based Metamaterials with Negative Poisson’s Ratio and Bistability,” *Phys. Rev. Lett.*, vol. 114, 2015.
[36] F. Fraternali *et al.*, “Dome-Shape Auxetic Cellular Metamaterials: Manufacturing, Modeling, and Testing,” vol. 6, p. 86, 2019.
[37] J. Conway, *The symmetries of things*, 1st ed. Taylor & Francis Inc, 2008.
[38] D. A. Huffman, “Curvature and Creases: A Primer on Paper,”

IEEE Trans. Comput., vol. C-25, no. 10, pp. 1010–1019, 1976.

[39] K. Miura, “A Note on Intrinsic Geometry of Origami,” *Res. Pattern Form.*, pp. 91–102, 1989.

[40] Z. Abel, D. Eppstein, J. Cantarella, T. C. Hull, and R. J. Lang, “Rigid Origami Vertices : Conditions and Forcing,” 2015.

3

An origami inspired transformable structure based on spherical symmetry groups

An origami inspired transformable structure based on spherical symmetry groups

Report by Ivar R. Nuijts
TU Delft, Department of Mechanical Engineering, Maritime Engineering and Materials Engineering (3mE)

Abstract- This paper presents a transformable metamaterial, inspired by origami. Generally, metamaterials are build up following the periodicity of Bravais lattices. This study aims to design a structure not following the Bravais lattices, but rather a different type of symmetry which tiles a sphere, in order to expand on current design studies. In this report the different types of spherical symmetries are discussed and the icosahedral symmetry group is used to design a theorical model. Then a prototype is designed and 3D-printed. Lastly the prototype is discussed and recommendations for further research are made.

Key words – spherical symmetries, auxetics, polyhedron, dilational metamaterial

1. Introduction

Metamaterials are materials with properties that are not found in naturally occurring materials, but rather engineered to have specific properties [1], [2]. Because these materials are man-made, they can have interesting counter-intuitive properties, such as a negative Poisson's ratio [2], [3]. Metamaterials with these properties are categorized as auxetic metamaterials. Auxetic metamaterials is a topic that has increased in popularity recently [2], [4], [5]. This is because of the interesting inventions that auxetic metamaterials made possible, for example, fasteners and rivets that expand widthways when pulled [6]. The possibilities are plenty, due to the fact that auxetics are structures or materials that when stretched, become thicker perpendicular to the applied force, which is not true for most materials. Auxetic structures that keep their exact shape while transforming are called dilational structures [7]. Multiple studies have been done on two-dimensional auxetic [6], [7], as well as three-dimensional auxetic [8]–[10]. Auxetic materials have found applications in a number of fields, such as sports [11] and nano-technology [12].

Fundamentally, most metamaterials are designed following the same pattern. First a unit cell is developed that exhibits auxetic behaviour. The unit cell is the smallest part in the material, or structure, that constitutes the repeating pattern [13]. This unit cell completely reflects the symmetry and structure of the entire material or structure, which is built up by repeated translations of this unit cell along the principal axes. These principal axes are defined by the nodes of the four different types of Bravais lattices in 2D, or the fourteen different types of Bravais lattices in 3D [14]. A Bravais lattice is a set of discrete points generated by discrete translations. Thus, most metamaterials are build up through periodic discrete translations of the unit cell.

Abovementioned approach makes it impossible to form every type of structure. Spheres are, for example, not able to be formed by Bravais lattices [15]. Although for a sufficiently small unit cell, a spherical structure can be

approximated using discrete translations, the curvature of spherical structures can never obtained via this method. To explain this, fig. 1 is used.

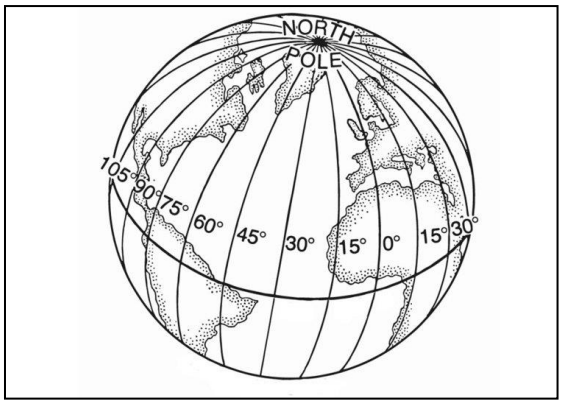

Figure 1. Sketched representation of the earth with different longitudes and the equator shown, from [16]

In the above figure a sketched representation of the globe is shown with different longitudes highlighted. These longitudes are parallel to each other at the equator, since they are all perpendicular to the equator, but converge to one point at both the North pole and South pole. These types of lines will never be acquired using Bravais lattices since they cannot be formed by discrete translations. Bravais lattices consist of sets of parallel lines, while meridians are only parallel at the equator. In other words, using the conventional methods of repeating units cells, three dimensional spherical structures cannot be obtained.

This study aims to create a dilational spherical shell based on the spherical symmetry groups. This way, a mechanical structure can be created that inherently fits a curved surface.

2. Spherical symmetry groups

Spherical symmetry groups is a topic which has not received as much attention as its planar counterpart, also known as the wallpaper groups [17]. One of the most prominent researchers in this field is John Conway, who has written the book '*The Symmetries of Things'* [18]. In this book Conway et al. explain intuitively what types of symmetries exist and how combining these results in different types of patterns. Repeating a pattern is done by either reflection or rotation, or a combination of these two. Reflection is mirroring an object with respect to a line. Rotation, or gyration, is defined by a circular movement of an object with respect to a fixed point. A translation is simply a rotation with the fixed point lying on the horizon, meaning at an infinite distance from the object. Thus, symmetries are based on only two types of transformations: reflections and rotations.

Conway introduces his own notations to classify different types of symmetries. For denoting reflections, or mirrors, he uses *(star) followed by the number, in red, representing the amount of mirror lines coming together in a single point. For example in fig 2. a *632 symmetry is shown. This means that there are three different types of intersections where the mirror lines meet. There are points where six, three or two mirror lines intersect. The area enclosed by the triangle with these intersections as vertices contains the motif of the structure. By repeating only the motif along the mirror lines, the whole structure is formed. The motif has the same functionality as the unit cell for planar engineering designs.

*Figure 2. A *632 symmetry of flowers in a plane is shown here. In red the mirror lines are shown and the red number denote the number of mirror lines meeting at a vertex, from [18].*

Rotations are expressed by blue numbers. In case the patterns consist of rotations and reflections, the signature of the patterns looks like this: [number of rotations] * [number of reflections], for example 3*2 which means a 3-fold rotation vertex and a 2-fold reflection vertex. Conway classifies two more types of transformations, however these will not apply to this research and are therefore not discussed.

Conway, and also others, provide mathematic proof to explain that there are exactly fourteen different types of possible isometries that tile a sphere [17]–[19] These types are seen in table 1. The table is an adaptation from [17]. This table shows the different types of symmetry groups, as well as the regular polyhedral corresponding to the platonic symmetry groups.

The different types can be categorised as parametric or platonic. Parametric groups, such as NN or *NN, where N can be any integer. An example of a parametric tiling where N=7 is seen in fig. 3. Parametric groups can be seen as globes with longitudes. The other type is platonic. These symmetries are named platonic since they are associated with the symmetry groups of the platonic solids: tetrahedron, cube, octahedron, dodecahedron and icosahedron. The dodecahedron and the icosahedron are each other's duals. The duality is because each face of the dodecahedron has five angles and three angles meet at any vertex, while the faces of the icosahedron all have three angles with five meeting at every vertex. Because these two platonic solids are each other's duals, they share the same symmetry groups. The same is true for the cube and octahedron. The tetrahedron is its own dual. This narrows down the total possible platonic symmetry groups.

Table 1: The fourteen types of spherical symmetries, classified by rotation or mirroring and parametric or platonic. The table is an adaption from [17].

	Polyhedron based on	Rotation based groups	Mirror based groups	Hybrid groups
Platonic groups	Icosahedron/ Dodecahedron	532	*532	
	Cube/ Octahedron	432	*432	
	Tetrahedron	332	*332	3*2
Parametric groups		NN N22	*NN *N22	N*2 N*× N*M

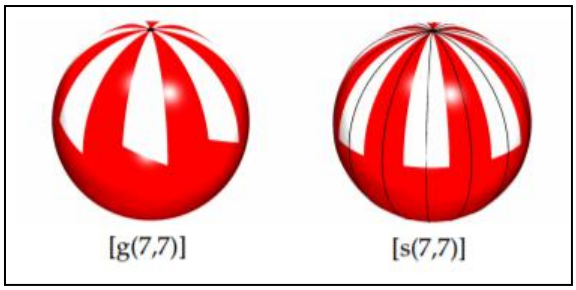

Figure 3. Two parametric groups, left is based on gyrations while right is based on reflections, from [17]

The designed structure needs to be a rigid mechanical system, modelling a spherical shell, thus dilational behaviour will be achieved through rigid body dynamics of surfaces hinged together. For accomplishing this behaviour the Japanese art of paperfolding, origami, has proven to be useful. From a mechanical viewpoint, origami has been considered as rigid body mechanisms, consisting of rigid plated connected by in-plane hinges [20]. Furthermore there have been multiple studies which use auxetic origami patterns for designing structures [21]–[24].

Because curved surfaces can, in general, not be folded without buckling or tearing, the simplification has been made that the spherical surface will be modelled as a polyhedron. Thus the surface will consist of multiple flat areas. For an adequate, and symmetrical, approximation of a sphere, the polyhedron benefits to be a regular polyhedron. Furthermore, regular polyhedral have the platonic symmetry groups based on them. Since the motifs will be designed flat instead of curved, it can be concluded that the platonic groups are more suitable for patterning with respect to the parametric groups, for this specific study. The platonic solids that most closely resemble a sphere are the icosahedron and the dodecahedron, simply because they consist of more faces and have a larger dihedral angle, which is the angle between two faces. This results in either the *532 or the 532 as a suitable symmetry group. This type of symmetry is, therefore, called icosahedral. The smallest repeated unit, or motif, of this symmetry is called the fundamental domain, the fundamental domain for any icosahedral symmetry is the face of the *Disdyakis Triacontahedron* (DT), see fig 4.

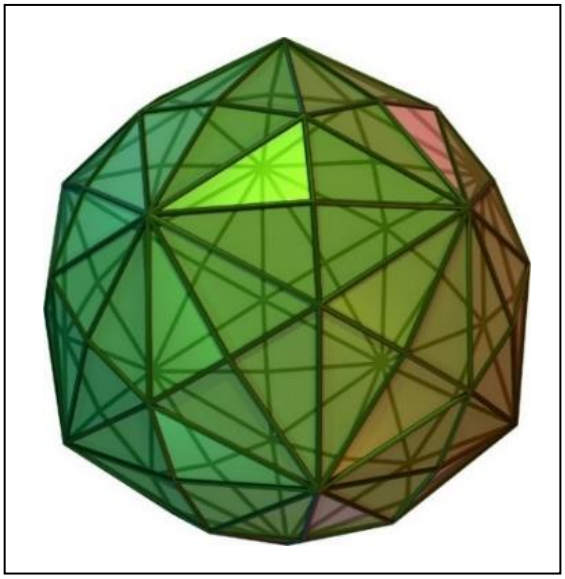

Figure 4. Figure of the Disdyakis Triacontahedron. A Catalan solid with 120 faces. The face of the Disdyakis Triacontahedron is the fundamental domain for the icosahedral symmetry group, from [25].

3. Construction of the structure

3.1 Polyhedral starting point

For this study the spherical shell will be modelled as a DT. This polyhedron is also known as the 'H*exakis Icosahedron, 'Decakis Dodecahedron'* and *kisRhombic Pentacontahedron*. These names all give information about the figure. '*Hexakis Icosahedron*', means having the icosahedron and dividing every face into six equal triangles. '*Decakis Dodecahedron'* in its turn means taking the dodecahedron and dividing every face into ten equals parts and '*Rhombic Pentacontahedron*' loosely means 30 rhombi, with a four-vertex fold in the middle of every rhombus. From these names the 532-

symmetry can be traced back, since these names imply that pentagons (5 axes of symmetry), triangles (3 axes of symmetry) and rhombi (2 axes of symmetry) are found on the surface of the DT. From the names it can also be deduced that the polyhedron has 120 equal triangles, which is also shown in fig. 4. With its 120 faces, the DT is the largest Catalan solid. A Catalan solid is a polyhedron which is face-transitive, but not vertex-transitive. This means that all the faces of the DT are equal, but the vertices are not. Drawing parallels with standard auxetic structures: two fundamental domains, since one is not a mechanism, of the DT acts as a unit cell, and the symmetry *532 acts as the Bravais lattices. Since the fundamental domain exists of just a plain triangle, there is no difference in a 532 or a *532 symmetry.

One might wonder if it is possible to create a closer resemblance of a sphere, with a smaller fundamental domain. In other words: applying crease lines to the fundamental domain, in order to create even smaller faces. Due to the specific angles of the fundamental domain, it is impossible to divide it into smaller congruent triangles. Because this study highlights the possibilities of using spherical symmetries, the choice is made to only have congruent triangles tiling up the whole spherical surface, making the DT the largest possible polyhedron.

A different point of attention regarding the fundamental domain, is that for creating a moving mechanism, cutting specific edges is inevitable. This is due to the fact that not all four fold vertices are possible. The only possible four fold vertex are three-to-one folds [23], [26], and even those are only possible in flat folding cases. A three-to-one fold of a four vertex means that one of the four folds is folded in opposite direction with respect to the other three. In this design study, where folding will be done on spherical surfaces, flat-folding is not possible. Furthermore, since symmetry is the focus, three-to-one folds are not well suited, Since a three-to-one fold results in unsymmetrical behaviour. In order to make different types of folds possible, specific edges need to be cut. In conclusion, starting with the DT and making every edge a fold inwards (valley fold), fold outwards (mountain fold), or a cut, the DT may be able to behave dilationally.

The DT can be seen as a set of twelve pentagons, (from the dodecahedron) or twenty triangles (from the icosahedron), see fig. 5. To achieve dilational behaviour, the choice is made to let either the pentagon or the triangle exhibit dilational behaviour and repeat that along the surface. This way it is ensured that the whole shell will behave symmetrical. Here the neighbouring conditions have to be factored in, such as that some edges needs to be cut and the kinematics between parts is not constrained. To determine what the best course of action is for the most dilational achievement, the pentagon model and the triangle model will be modelled in Matlab.

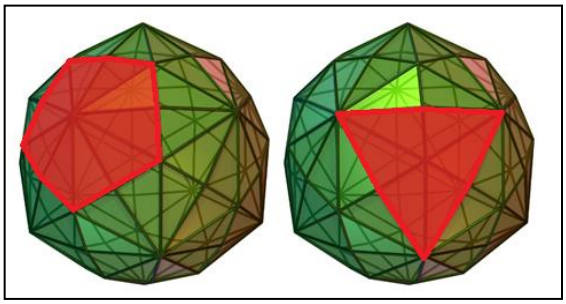

Figure 5. The Disdyakis Triacontahedron with the underlying pentagon highlighter left and the underlying triangle highlighted right, from [25].

3.2 Modelling

In order to determine what will be the best course of action, using a triangular structure as building block or a pentagonal structure, both these

structures will be discussed separately. The process and the results of these are found in Appendix A. The values used for constructing the plots are based on the unit-edge-length of the Truncated Icosidodecahedron [27]. Parts of the DT which form a triangular or pentagonal structure were modelled in Matlab. The pentagonal structure has a larger projected surface decrease with respect to the triangular surface. Based on this result, it is concluded that the pentagonal structure will function as a building block and the structure will be built by connecting twelve pentagonal structures.

This is done by first modelling one side of the pentagonal structure. The assumption is made that all five sides of the pentagonal structure transform in the same manner, meaning that a 5 fold rotational symmetry is applied to the pentagon, see fig. 6 for the modelled pentagonal structure. When the pentagon behaves as desired, it functions as the unit cell for the whole polyhedron. The entire structure is built through rotation and translation of the unit cell.

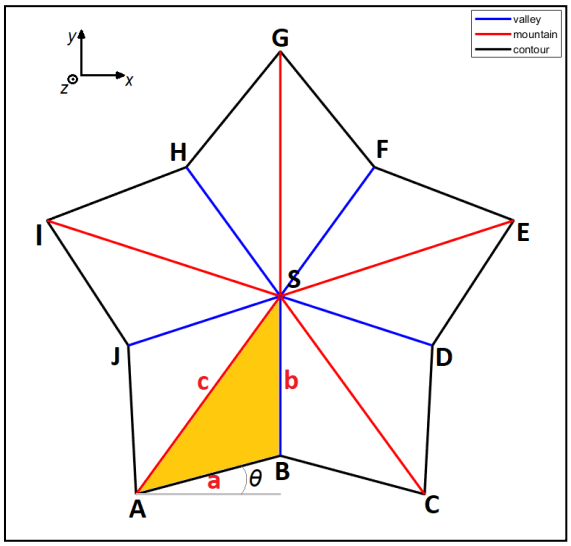

Figure 6. Schematic overview of the pentagonal model projected in the xy-plane with all imporant vertices and edges labelled

3.3 Design adjustments

For any position of the model which is not its initial state, it becomes evident that the connected edge will need to open up. See fig. 6 as illustration.

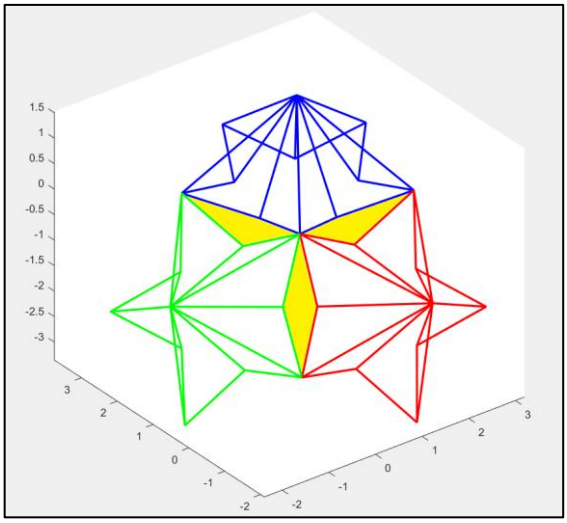

Figure 7. Schematic overview of three pentagonal structures in correct orientation in a configuration for which theta is not equal to zero. In yellow areas are depicted which are created by the contraction of each individual pentagon.

This happens since the edge points of each pentagon move away from one another. This results in an open space, which is depicted by the yellow area's in fig. 7. This results in the pentagons being connected only by single points, which are not sufficiently strong due to the minimal contact area. The pentagons need extensions which will transform point contact to line contacts to ensure a fundamentally strong connection.

4. Methods

The full model is built by drawing the pentagonal structure and connecting twelve of these together. The pentagons are 3D-printed in a flat plane and then later connected to itself and other pentagons. The materials is PLA, and the used printer is the Prusa MK2. The model is drawn in SolidWorks with a thickness of 3 mm. In fig. 8 a top view of one flat-folded face of the model is shown. This model consists of the

pentagonal structure with appendices that function as line contacts between the pentagons. The model shows puzzle like structures which are required for smooth connections between the pentagons, but also for closing the pentagon itself. The printer is instructed to pause twice, after printing a thickness of 0.5mm and 2.75mm, to apply a layer of netting. Netting is used as hinge material and the holes of the netting ensure that the plastic layers will melt together. By selectively cutting the top or bottom layer of the netting, mountain-valley assignments are made. This ensures that the hinges between the fundamental domains only allow movement along one direction. From the line contacts the twelve pentagons can be connected together. In appendix C more detail is given of this process, as well as figures of the SolidWorks model showing its dimensions.

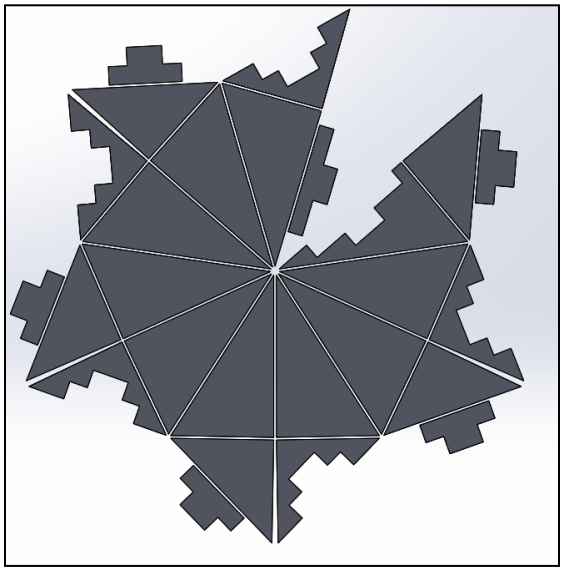

Figure 8. Top view of the pentagonal structure. Puzzle like appendices are added to function as line contacts between the pentagons.

5. Degrees of freedom

In order to have some insight on how to actuate the model, or to know how easily the transformation will be, the total degrees of freedom of the system was determined. The degrees of freedom are determined through a multi-body analysis and checked with determining the nullspace of the Jacobian with the help of Matlab [28]. The full explanation is found in Appendix B. Both methods yield the same result: 33 DoF's for the total structure.

6. Results

The whole DT consists of twelve pentagons. By the use of translations, rotations and mirroring the whole DT is plotted, based from a single pentagonal structure. See fig. 9 for the initial dilated state and fig. 10 for the final folded state.

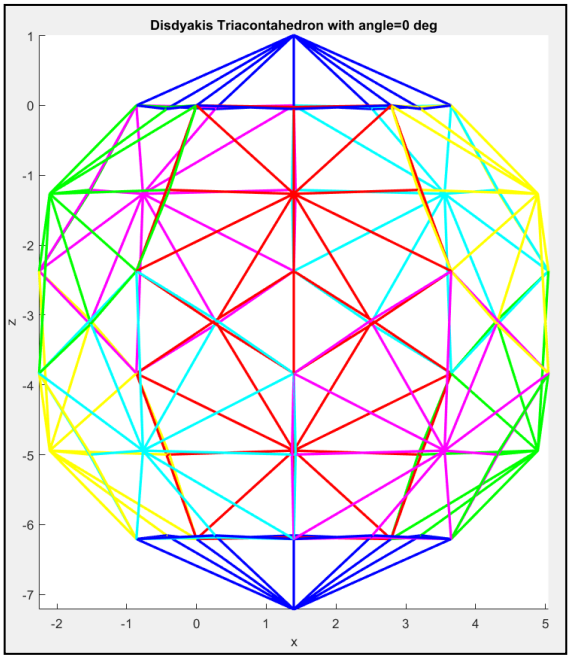

Figure 9. Plot of the final model in initial state, every pentagonal structure is coloured differently with respect to its neighbour.

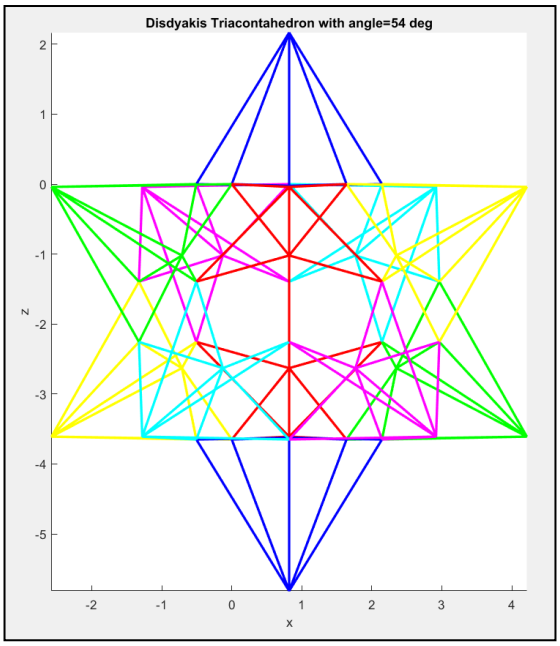

Figure10. Plot of the final model in final state, every pentagonal structure is coloured differently with respect to its neighbour.

From figures 9 and 10, it shows that the movement resembles symmetrical transformation, which is desired. If a specific set of points is chosen, it shows that a dodecahedron transforms into a smaller dodecahedron. In the dilated state, certain points are pushed outwards, which is not a problem for this design study. Since this study's main focus is to explore symmetrical symmetries and the possibilities surrounding them, this is not a problem which affects the functionality of the design.

A grid is printed on which the prototype is shown in both extreme positions. From this the extent of the contraction is indicated, see fig. 11. Positioning the prototype in both extreme states was proven very difficult to do. Left in fig. 11 the begin state is shown to the extent possible, same as for the right picture where the final state is show.

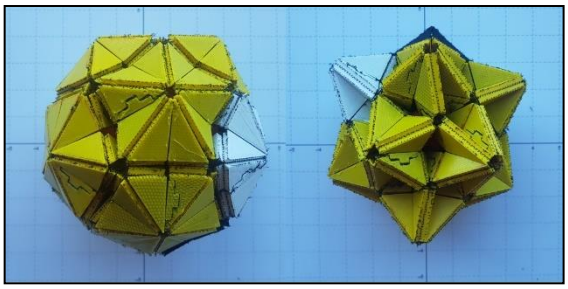

Figure 11. Picture showing the protype in the initial state (left) and the final state (right) placed on a grid.

To show the extents of the transformation, fig. 12 is used. Here the contour, in red, of the begin state is shown over the final state, which also has its contour highlighted in red.

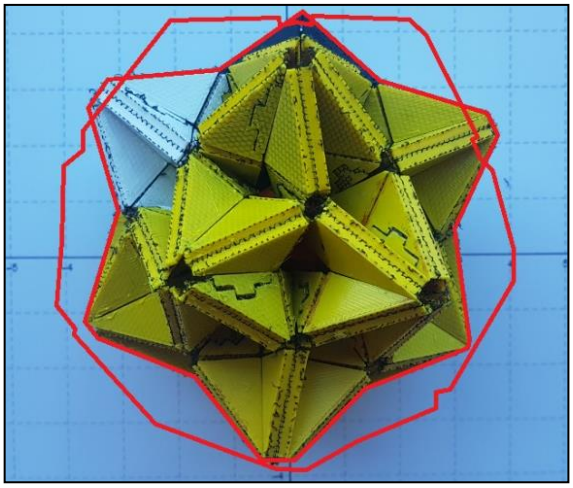

Figure 12. Picture overlaying the contours of the initial and the final state.

It shows that due to the symmetry groups and the mountain-valley assignments of pentagonal-model the protype transforms to a shape which is in accordance with the Matlab plots, shown in fig. 8 and fig.9.

From fig. 12 it is not clear to which extent dilational movement is achieved. To determine this, the enclosed dodecahedron is used. The face of the enclosed dodecahedron is made up of the five vertex points of the individual pentagonal structure, see fig. 13. The volume of this dodecahedron in initial dilated state is equal to circa 88.34, while the volume of the final state is 20.97, meaning a volume reduction of 76.3% is reached. The values are

based on the dimensions given in [27], where no units were used.

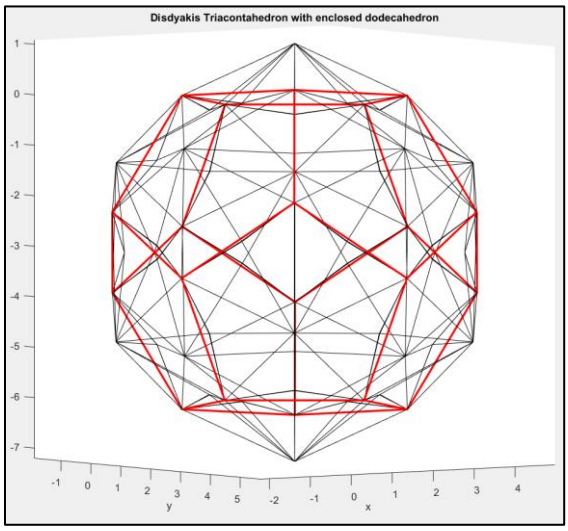

Figure 13. Disdyakis triacontahron shown in black with the enclosed dodecahedron shown in red.

As an additional remark: the netting works well as hinge. It has no fatigue and enough play to function correctly even if the puzzle pieces aren't exactly lined up correctly. The only downside to this netting is that it has almost no stiffness. This results in that the structure is difficult to contain in a specific state, since the hinges will always allow the structure to fall back into a static equilibrium. This makes it unreliable to determine if the build prototype has 33 DoF's. A balloon was fitted inside the prototype to easily put the prototype in the beginning state.

7. Discussion

Likely, dilational efficiency could be increased by applying crease lines to the fundamental domain, in order to create even smaller faces. This however, is associated with different problems. To explain, fig. 14 is used. Fig. 14 is a plot of two fundamental domains of the DT. Same as in the DT, these two faces are not in the same plane, there is an angle between them not equal to 180°. The blue and red arrow represent the normal vector of the two faces. If the fundamental domain needs to be split up into smaller faces, then fold lines need to be applied to the fundamental domain that extend to the edges. For any infinitesimal crease in the fundamental domain on the edge, the edge will move perpendicular to the surface. For the left fundamental this is following the blue arrow, for the right this is following the red arrow. The middle edge is an edge for both the left and the right fundamental domain. This edge will thus need to move following both the blue and the right normal, which is not possible unless the two break free from each other. In conclusion, any fold lines that create smaller area's than the fundamental will results in tearing of the material, or cutting open edges. Which is an consideration one needs to make. In addition it would add to the complexity of the model since more cut edges results in more point contacts and thus extra connections would be needed just as in the current model.

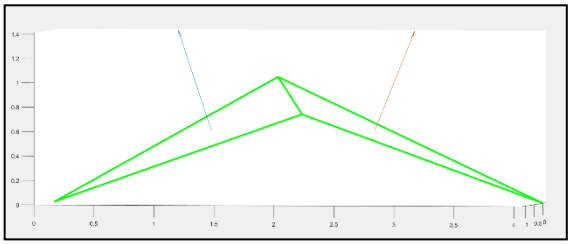

Figure 14. Schematic representation of two fundamental domains of the DT under an angle, the normals of the faces are shown as a blue and red arrow.

This study used the *532 symmetry as building block for creating a prototype, however the octahedral symmetry group (*432) would work in a similar manner, albeit with less faces. Parametric symmetry groups have their own benefits, that being that the number of parts to form a structure can be chosen and is not limited to the faces of a polyhedron.

Looking at the final model it is seen that the centres of each individual pentagon point outwards. Since the underlying objective is not to have a perfect sphere

in every state, but rather to investigate whether or not new types of symmetries are plausible for design studies, this is not a detraction.

However, if one would has an application in mind where this would a problem, it is possible to flip the pentagons upside down. This implies that the centres of the pentagons move inward, rather than outward. This is illustrated in fig. 15 and 16. From this illustration, It also shows that the resulting mechanism does not resemble a sphere as well as the design presented in this paper.

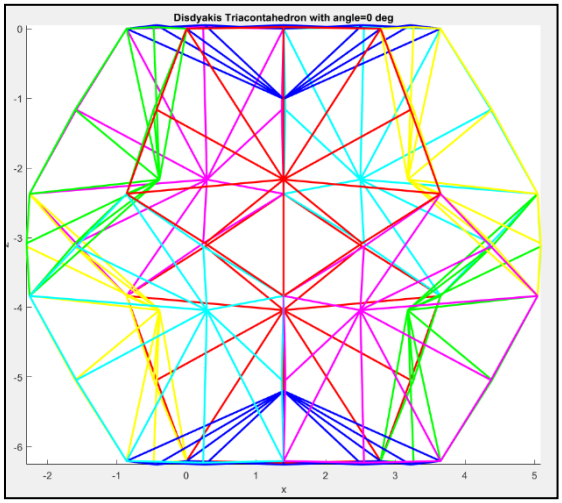

Figure 15. Matlab plot of the model in initial state with the pentagonal parts pointed inward rather than outward.

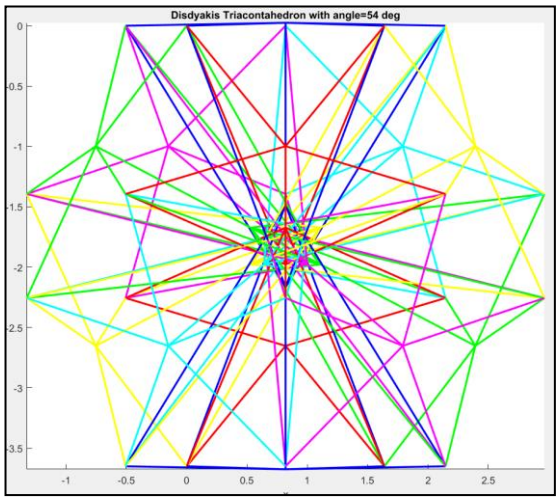

Figure 16. Matlab plot of the model in final state with the pentagonal parts pointed inward rather than outward.

The fitted balloon can also be seen as an actuator with one DoF. Due to that the balloon presses against the puzzle pieces that are pointed inward, the whole prototype moves to its beginning position. This principle could also be reversed. A connection could be made from these inward pointing puzzle pieces to the centre of the prototype, where all these connections would meet. If this point could be actuated properly, the whole system would only have one DoF and thus much more easily actuated. This is an interesting idea for further research.

The 33 DoF's make actuating the model a difficult task. For further research an efficient way to actuate these mechanisms can be developed, which makes use of the symmetric properties of these kinds of structures, this may result in needing much less actuators than 33.

8. Conclusion

This study illustrated the possibilities of using different types of symmetry-groups, other than the known Bravais lattices, when creating structures based from a unit cell. From an engineering perspective, origami is a type of rigid body mechanics, making it possible to model the kinematics of the structure. By dividing the spherical structure into parts that can be placed in a flat plane, they can be easily fabricated by, for example, 3D printing.

Spherical symmetries, both platonic and parametric, could pose as a solution for creating new structures. In this study, a new origami inspired spherical dilational metamaterial was created, based on a platonic symmetry-group. From the results it shows that the enclosed dodecahedron of the model initially has a volume of 88.34 and for the end state a volume of 20.97. Meaning the model undergoes a

volume reduction of 76.3% from beginning to end state.

Bibliography

[1] R. S. Kshetrimayum, “A brief intro to metamaterials,” *IEEE Potentials*, vol. 23, no. 5, pp. 44–46, 2004.

[2] A. A. Zadpoor, “Mechanical meta-materials,” *Mater. Horizons*, vol. 3, no. 5, pp. 371–381, 2016.

[3] Y. Liu and H. Hu, “A review on auxetic structures and polymeric materials,” *Sci. Res. Essays*, vol. 5, no. 10, pp. 1052–1063, 2010.

[4] X. Yu, J. Zhou, H. Liang, Z. Jiang, and L. Wu, “Mechanical metamaterials associated with stiffness, rigidity and compressibility: A brief review,” *Prog. Mater. Sci.*, vol. 94, pp. 114–173, May 2018.

[5] Y. Zárate *et al.*, “Elastic metamaterials for tuning circular polarization of electromagnetic waves,” *Sci. Rep.*, vol. 6, 2016.

[6] K. E. Evans, “Auxetic polymers: a new range of materials.”

[7] G. W. Milton, “New examples of three-dimensional dilational materials,” *Phys. Status Solidi Basic Res.*, vol. 252, no. 7, pp. 1426–1430, 2015.

[8] S. Babaee, J. Shim, J. C. Weaver, E. R. Chen, N. Patel, and K. Bertoldi, “3D soft metamaterials with negative poisson’s ratio,” *Adv. Mater.*, vol. 25, no. 36, pp. 5044–5049, 2013.

[9] G. W. Milton, “Complete characterization of the macroscopic deformations of periodic unimode metamaterials of rigid bars and pivots,” 2012.

[10] M. Kadic, T. Bückmann, N. Stenger, M. Thiel, and M. Wegener, “On the practicability of pentamode mechanical metamaterials,” *Appl. Phys. Lett.*, vol. 100, no. 19, p. 191901, May 2012.

[11] M. Sanami, N. Ravirala, K. Alderson, and A. Alderson, “ScienceDirect Auxetic materials for sports applications,” *Procedia Eng.*, vol. 72, pp. 453–458, 2014.

[12] M. Kadic, T. Bückmann, R. Schittny, and M. Wegener, “Metamaterials beyond electromagnetism,” *Rep. Prog. Phys*, vol. 76, pp. 1–34, 2013.

[13] X. Yu, J. Zhou, H. Liang, Z. Jiang, and L. Wu, “Mechanical metamaterials associated with stiffness, rigidity and compressibility: A brief review,” *Prog. Mater. Sci.*, vol. 94, pp. 114–173, 2018.

[14] Wikipedia contributors, “Cite This Page - Wikipedia,” *Wikipedia, The Free Encyclopedia.* [Online]. Available: https://en.wikipedia.org/w/index.php?title=Special:CiteThisPage&page=Crystal_structure&id=890894105. [Accessed: 04-Apr-2019].

[15] “Cite This Page - Wikipedia,” *Wikipedia, The Free Encyclopedia.*, 2019. [Online]. Available: https://en.wikipedia.org/w/index.php?title=Special:CiteThisPage&page=Bravais_lattice&id=877311057. [Accessed: 04-Apr-2019].

[16] “Kleurplaat lengtegraden - Afb 13197.” [Online]. Available: https://www.schoolplaten.com/kleurplaat-lengtegraden-i13197.html. [Accessed: 04-Apr-2019].

[17] J. Van De Craats, “Symmetric Spherical and Planar Patterns,” 2011.

[18] J. Conway, *The symmetries of things*, 1st ed. Taylor & Francis Inc, 2008.

[19] J. van de Craats, “Symmetrie op de bol en in het vlak.”

[20] Z. Abel, D. Eppstein, J.

Cantarella, T. C. Hull, and R. J. Lang, “Rigid Origami Vertices : Conditions and Forcing,” 2015.
[21] B. Gin-Ge Chen *et al.*, “Topological Mechanics of Origami and Kirigami,” *Phys. Rev. Lett.*, vol. 116, 2016.
[22] M. Eidini, “Zigzag-base folded sheet cellular mechanical metamaterials,” *Extrem. Mech. Lett.*, vol. 6, pp. 96–102, 2016.
[23] K. Miura, “A Note on Intrinsic Geometry of Origami,” *Res. Pattern Form.*, pp. 91–102, 1989.
[24] Y. Nishiyama, “Miura Folding: Applying Origami to Space Exploration.”
[25] “Wikimedia Commons.” [Online]. Available: https://commons.wikimedia.org/wiki/Main_Page. [Accessed: 28-Mar-2019].
[26] D. A. Huffman, “Curvature and Creases: A Primer on Paper,” *IEEE Trans. Comput.*, vol. C-25, no. 10, pp. 1010–1019, 1976.
[27] “Disdyakis Triacontahedron.” [Online]. Available: http://dmccooey.com/polyhedra/DisdyakisTriacontahedron.html. [Accessed: 21-Feb-2019].
[28] R. G. Hutchinson and N. A. Fleck, “The structural performance of the periodic truss,” *J. Mech. Phys. Solids*, vol. 54, pp. 756–782, 2006.

4

Discussion

In this chapter certain design choices will be reflected upon and some ideas for further research will be presented as well.

This design study very early on drew inspiration from origami. This was a choice by the author, since the wide range of possibilities made it necessary to make design choices. The choice of origami made it necessary to stick to rigid body mechanics as requirements for designing the sphere. For further research, one could explore different engineering principles to design spherical auxetic structures, for instance: compliant mechanisms or elastic materials.

In chapter 3 "*An origami inspired transformable structure based on spherical symmetry groups"* the motivations for choosing a *532 symmetry-group as pattern for the design were stated and for this study this was the only symmetry-group explored. It would be interesting to explore more platonic symmetry-groups. Such as the groups based on the cube and octahedron: *432, 432 or the tetrahedron: *332, 332, which would result in a *disdyakis dodecahedron* and *triakis tetrahedron* respectively. These however, resemble a spherical structure much less than the disdyakis triacontahredon, due to a lower face count. The symmetry-group perhaps need not even be platonic, a parametric symmetry-group could have their application in other designs.

Due to limited resources the fabrication possibilities were restricted. Using the 3D printer for fabrication proved to be the best option for building a prototype. If it were possible on campus, a laser-cutter or paper-cutter could also be beneficial. The prototype could be made of cardboard or paper, and double-sided tape could be used instead of the netting. This would result in a much thinner model, but perhaps also more easily puzzled together and fabricated faster. The 3D-printing process took up four whole days.

The model could have been simplified by using tape as hinge, instead of netting and puzzle-like pieces. This, however, would make the prototype less intricate. The current prototype added more depth and design to the study. The main focus of the prototype was to test the dilational behaviour, but due to some inventive design choices: netting as hinge and puzzling the pentagons together, the prototype received another layer of ingenuity which added to the complexity and innovativeness of the study.

It has previously been stated that the icosahedron and dodecahedron are each other's duals and thus share the same symmetry-group, meaning it would also be possible to construct the prototype out of 20 triangles, which is also mentioned in appendix A, where the choice for the pentagon was substantiated. As an alternative design, the triangle could be taken as the basis of the model, instead of the pentagon. This would result in 15 DoF's for the total structure, since the triangle has 3 internal DoF's, with respect to the 7 of the pentagon.

5

Conclusion

This thesis developed an origami inspired dilational metamaterial. The model is based on spherical symmetries, specifically the icosahedral symmetry-group. This distinguishes it from the current state-of-the-art of metamaterials, which are all formed through discrete translations along the lattice vectors of different Bravais lattices.

The thesis started with a literature survey where certain mechanical metamaterials were introduced and discussed, with the focus on auxetic metamaterials, as well as origami patterns that behave in an auxetic manner. Origami was stated to be useful to drawn inspiration from, especially in a preliminary stage, because any idea for a pattern could easily be tested with a piece of paper. The goal of this survey was to state the current research gap, which is that all metamaterials are constructed through discrete translations of the unit cell, making it impossible to form spherical structures.

In chapter 3 this concept is further developed by listing the existing spherical symmetry-groups and categorizing them as either parametric or platonic. The platonic symmetry-groups were proven to be more suited for this specific study, with the platonic polyhedrons linked to them. The model was then constructed in Matlab, drawn in SolidWorks and fabricated in PLA with a Prusa MK2 3D-printer. The results of the prototype were in compliance with the theoretical model.

This design study developed a never seen before dilational mechanical metamaterial based on a spherical symmetry-group, with 33 DoF's. One degree of freedom results in perfect dilational behaviour from beginning to final state causing a volume reduction of the enclosed dodecahedron of 76,3%.

The results of this study made it possible to project auxetics fittingly on curved surfaces, by means of spherical symmetry-groups.

Bibliography

[1] P. M. Reis, H. M. Jaeger, and M. van Hecke, “Designer Matter: A perspective,” *Extrem. Mech. Lett.*, vol. 5, pp. 25–29, 2015.

[2] X. Hou and V. V. Silberschmidt, “Metamaterials with Negative Poisson’s Ratio: A Review of Mechanical Properties and Deformation Mechanisms,” in *Mechanics of Advanced Materials*, Springer, Cham, 2015, pp. 155–179.

[3] R. S. Kshetrimayum, “A brief intro to metamaterials,” *IEEE Potentials*, vol. 23, no. 5, pp. 44–46, 2004.

[4] Y. Zárate *et al.*, “Elastic metamaterials for tuning circular polarization of electromagnetic waves,” *Sci. Rep.*, vol. 6, 2016.

[5] M. Kadic, T. Bückmann, N. Stenger, M. Thiel, and M. Wegener, “On the practicability of pentamode mechanical metamaterials,” *Appl. Phys. Lett.*, vol. 100, no. 19, p. 191901, May 2012.

[6] M. Sanami, N. Ravirala, K. Alderson, and A. Alderson, “ScienceDirect Auxetic materials for sports applications,” *Procedia Eng.*, vol. 72, pp. 453–458, 2014.

[7] K. E. Evans and A. Alderson, “Auxetic materials: Functional materials and structures from lateral thinking!,” *Adv. Mater.*, vol. 12, no. 9, pp. 617–628, 2000.

[8] A. A. Zadpoor, “Mechanical meta-materials,” *Mater. Horizons*, vol. 3, no. 5, pp. 371–381, 2016.

[9] “Cite This Page - Wikipedia,” *Wikipedia, The Free Encyclopedia.*, 2019. [Online]. Available: https://en.wikipedia.org/w/index.php?title=Special:CiteThisPage&page=Bravais_lattice&id=877311057. [Accessed: 04-Apr-2019].

[10] G. F. Méjica and A. D. Lantada, “Comparative study of potential pentamodal metamaterials inspired by Bravais lattices,” *Smart Mater. Struct.*, vol. 22, no. 11, 2013.

[11] J. Van De Craats, “Symmetric Spherical and Planar Patterns,” 2011.

[12] J. Conway, *The symmetries of things*, 1st ed. Taylor & Francis Inc, 2008.

[13] M. Eidini, “Zigzag-base folded sheet cellular mechanical metamaterials,” *Extrem. Mech. Lett.*, vol. 6, pp. 96–102, 2016.

[14] B. Gin-Ge Chen *et al.*, “Topological Mechanics of Origami and Kirigami,” *Phys. Rev. Lett.*, vol. 116, 2016.

[15] Y. Nishiyama, “Miura Folding: Applying Origami to Space Exploration.”

Appendices

The first appendix consists of the mathematical models of the triangular and pentagonal structures. This is the foundation of the Matlab code. The second appendix consists of the Degree of Freedom calculations for the triangular and pentagonal structures as well as the full model. The third appendix shows pictures of the fabrication process. The last appendix shows the used Matlab scripts.

Contents

Appendix A: Triangular and Pentagonal structure mathematical model

A.1 The triangular structure

In order to better understand the kinematics and the geometry of the structure, the portions of the Disdyakis Triacontahedron (DT) that represent the pentagon and the triangle are modelled in Matlab. First the triangle is modelled. All the vertices are labelled as followed, see figure 7. The vertices are labelled by the capital letter A through F and S. The edges of the FD are labelled with a, b and c, with a being the shortest edge and c the longest. The edges have a blue, red or black colour. The black colour denotes the contour of the structure and these edges will later be examined. The blue colour shows the 'valley' folds, meaning those foldlines are folded inward. The red lines represent the 'mountain' folds, meaning the folds are outwards. A single fundamental domain is coloured yellow. Fig. 1 shows a projection in the xy-plane and the angle θ (theta) represents the angle between AB and the x-axis and is used to describe the other points with respect to A, together with the constants: a, b and c. The values of a, b and c are based on the Truncated Icosidodecahedron, which is the dual of the DT. The Truncated Icosidodecahedron is an Archimedean solid, meaning that every edge has the same length, which is determined to be 1 for this study. Based on this edge length, the vales of a, b and c are determined.

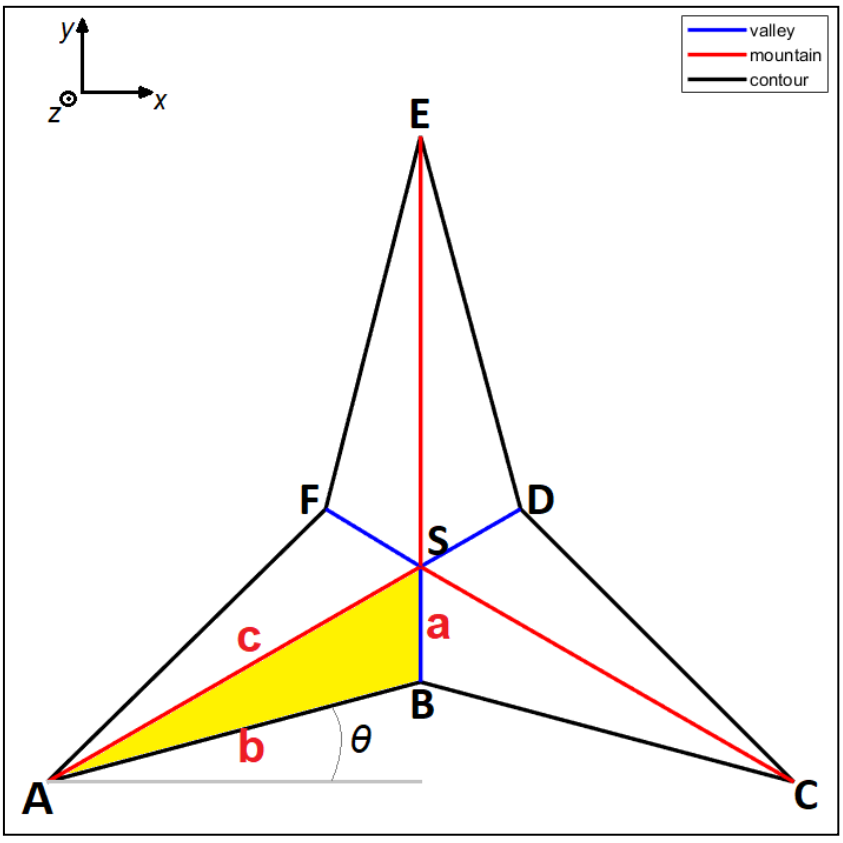

Figure 1. Schematic overview of the triangle model projected in the xy-plane with all imporant vertices and edges labelled

Fig. 2 and fig. 3 show the same triangle in the yz-plane and the xz-plane respectively.

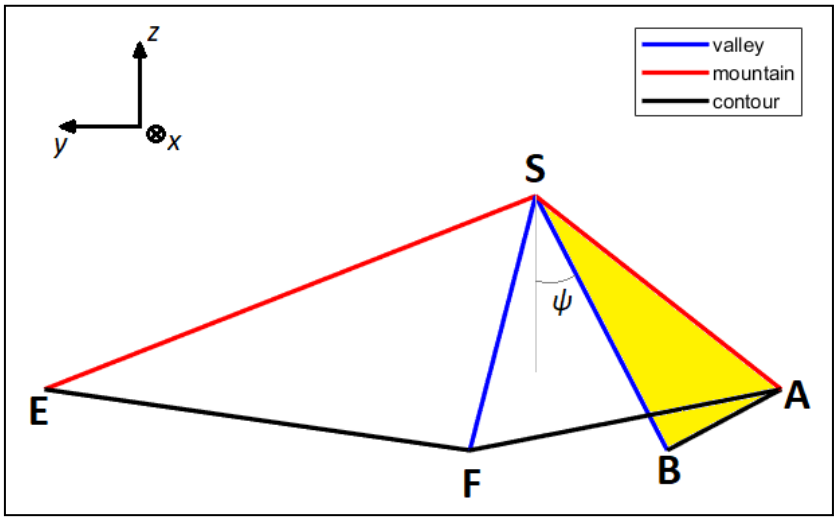

Figure 2. Schematic overview of the triangle model projected in yz-plane. This orientation displays angle psi which will be used to express point S

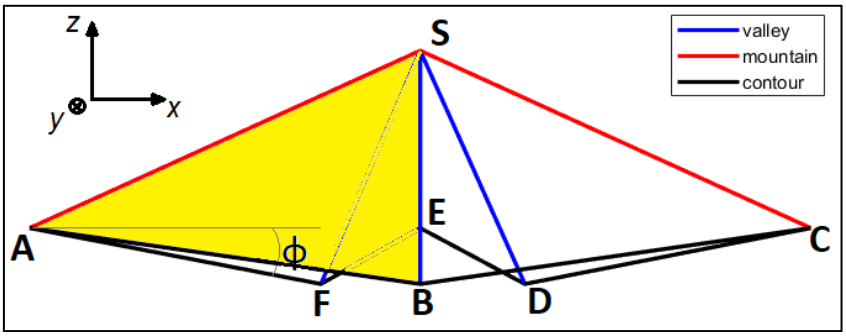

Figure 3. Schematic overview of the triangle model projected in xz-plane. This orientation displays angle phi which determines the displacement in the z-direction of the points.

Using the angles θ, φ, ψ the coordinates of B through F and S can be expressed with respect to A. Angle θ lies in the xy-plane, φ lies in the xz-plane and ψ lies in the yz-plane, as is illustrated below. Point A is fixed in the origin, meaning the coordinates of A are:

$$A = \begin{bmatrix} 0 \\ 0 \\ 0 \end{bmatrix}$$

By fixing the y- and z-coordinate of C and the z-coordinate of E, the whole structure is fixed in space. The points B through F are expressed in the angles and the constants a, b, c.

$$B = \begin{bmatrix} bcos(\theta)cos(\phi) \\ bsin(\theta)cos(\phi) \\ -bsin(\phi) \end{bmatrix}$$

The assumption is made that triangle ΔABC is a isosceles triangle, meaning the movement is symmetrical. This assumption is extended for the whole structure, meaning $\Delta AFE$and ΔCDE are also assumed to be isosceles. Furthermore it is assumed that if $\angle BAC = \theta$ then $\angle EAF = \theta$ as well. This assumption is extend to state $\angle DCE = \theta$

too, however this assumption will later be validated. Using the assumptions and geometry, the following points can be expressed as:

$$C = \begin{bmatrix} 2bcos(\theta)cos(\phi) \\ 0 \\ 0 \end{bmatrix}$$

$$D = \begin{bmatrix} C(1) - bsin(\theta + \frac{\pi}{6})cos(\phi) \\ C(2) + bcos\left(\theta + \frac{\pi}{6}\right)cos(\phi) \\ C(3) - bsin(\phi) \end{bmatrix} = \begin{bmatrix} 2bcos(\theta)cos(\phi) - bsin(\theta + \frac{\pi}{6})cos(\phi) \\ bcos\left(\theta + \frac{\pi}{6}\right)cos(\phi) \\ -bsin(\phi) \end{bmatrix}$$

$$E = \begin{bmatrix} D(1) - bcos(\theta + \frac{\pi}{3})cos(\phi) \\ D(2) + bsin\left(\theta + \frac{\pi}{3}\right)cos(\phi) \\ C(3) + bsin(\phi) \end{bmatrix}$$

$$= \begin{bmatrix} 2bcos(\theta)cos(\phi) - bsin\left(\theta + \frac{\pi}{6}\right)cos(\phi) - bcos\left(\theta + \frac{\pi}{3}\right)cos(\phi) \\ bcos\left(\theta + \frac{\pi}{6}\right)cos(\phi) + bsin\left(\theta + \frac{\pi}{3}\right)cos(\phi) \\ 0 \end{bmatrix}$$

F is expressed with respect to A:

$$F = \begin{bmatrix} bsin\left(\theta + \frac{\pi}{6}\right)cos(\phi) \\ bcos\left(\theta + \frac{\pi}{6}\right)cos(\phi) \\ -sin(\phi) \end{bmatrix}$$

Lastly S is expressed with respect to B:

$$S = \begin{bmatrix} B(1) \\ B(2) + asin(\psi) \\ B(3) + acos(\psi) \end{bmatrix} = \begin{bmatrix} bcos(\theta)cos(\phi) \\ bsin(\theta)cos(\phi) + asin(\psi) \\ -bsin(\phi) + acos(\psi) \end{bmatrix}$$

Now that the coordinates of the whole structure are defined, constraints can be defined. Both constraints involve point S, S is described with respect to B, but the distance between S and A remains constant, namely c. Even so the distance between S and D is the constant a. Using this, the constraints can be written as:

$$eq1: \quad d(A,S) - c = 0$$
$$eq2: \quad d(D,S) - a = 0$$

More constraints can be added, for example the distance between E and S also being c, however this will over-constrain the system and are thus not wanted. Since three angles are needed to express all the points of the system, and two independent constraints are imposed, this means that the system will be a one degree of freedom (DoF) mechanism. For a given value θ and the two constraint equations, values for ψ

and φ are determined and the structure can be plotted for any $0 \leq \theta \leq \frac{\pi}{6}$. See fig. 4 for $\theta = \frac{\pi}{12}$.

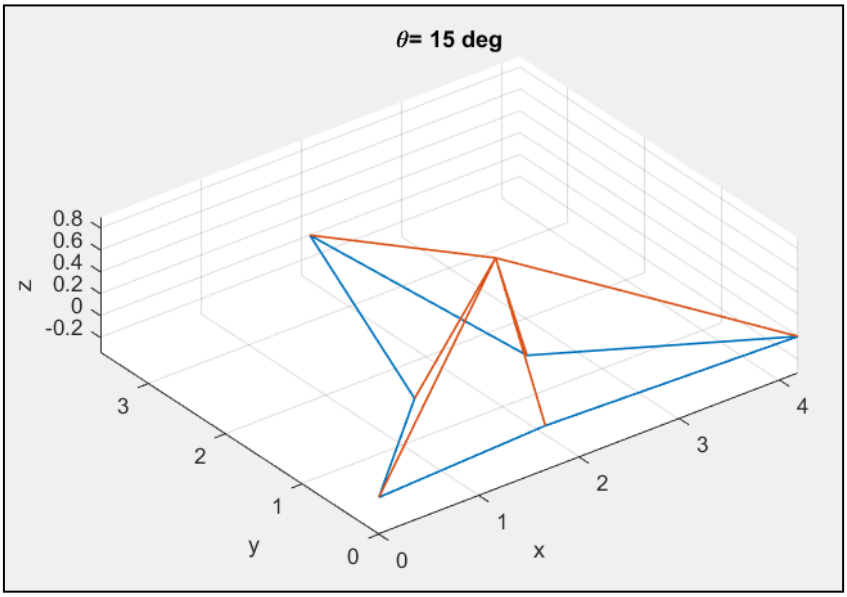

Figure 4. Plot of the triangle model for theta=15°

From this it is possible to determine what the maximum contraction will be, and what the effective area decrease is. The projected area in the xy-plane is determined by:

$$A(\Delta ACE) = \frac{1}{2} * 2b\cos(\theta)\cos(\psi) * \left(b\cos\left(\theta + \frac{\pi}{6}\right)\cos(\phi) + b\sin\left(\theta + \frac{\pi}{3}\right)\cos(\phi)\right)$$

For the initial state it follows:

$$\theta = 0, \psi = 0.0416\, rad, \text{thus } A(\Delta ACE) = 8.2940$$

For the end state it holds:

$$\theta = \frac{\pi}{6} rad, \psi = 0.0176\, rad, \text{ thus } \quad A(\Delta ACE) = 6.2294$$

Yielding an area deduction of almost 25 percent.

$$\frac{6.2294 - 8.2940}{8.2940} * 100\% = -24.9\%$$

In the assumption that angle C and E are not theta, more variables are needed. The only point which is not describable from A with the symmetry assumption is point D. $\angle DEB = \angle DCB = \zeta$ instead of θ. Angle ψ is replaced by angle δ and angle φ replaced by ε. The goal is to let Matlab find the angles instead of assuming symmetry. Because three new angles are introduced, new constraint equations need also be necessary. These constraints all rely on point D.

$$eq3: \quad d(C,D) - b = 0$$
$$eq4: \quad d(D,E) - b = 0$$

$$eq5: \qquad d(D,S) - a = 0$$

Letting Matlab solve this set of equations, with known angles theta, phi and psi, for unknown angles zeta, delta and epsilon yields values for these angles that have a difference of circa 10^{-15} degrees when compared to complete symmetry. This result shows that symmetry may be assumed.

A.2 The pentagonal structure

The pentagonal structure is a more intricate mechanism in contrast to the triangular counterpart, since the model has more degrees of freedom. The figure below shows a sketch of the model with the lengths of the sides and the angles used for describing the geometry, same as the triangle model. However, more angles are needed. The points A, C, E, G and I are assumed to behave symmetrically. Furthermore if four points are fixed, the fifth point is fixed as well. Thus, four different theta angles are needed. Every theta needs its own phi angle, thus four phi angles are needed. Lastly, one psi is needed to express S. Thus nine angles are needed for expressing the geometry of the system. Figures 5, 6 and 7 are used to express what the model should look like and how its coordinates are labelled for Matlab.

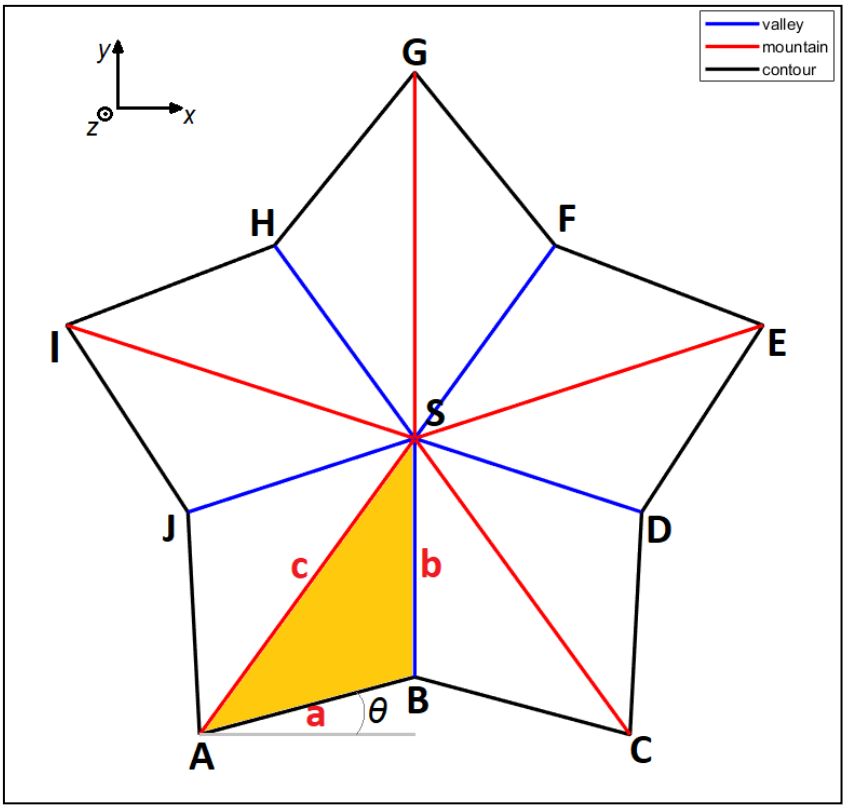

Figure 5. Schematic overview of the pentagonal model projected in the xy-plane with all imporant vertices and edges labelled

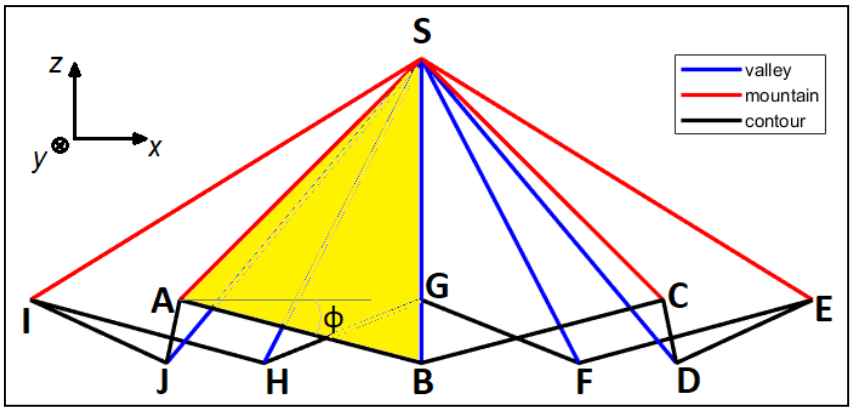

Figure 6. Schematic overview of the pentagonal model projected in xz-plane. This orientation displays angle phi which determines the displacement in the z-direction of the points.

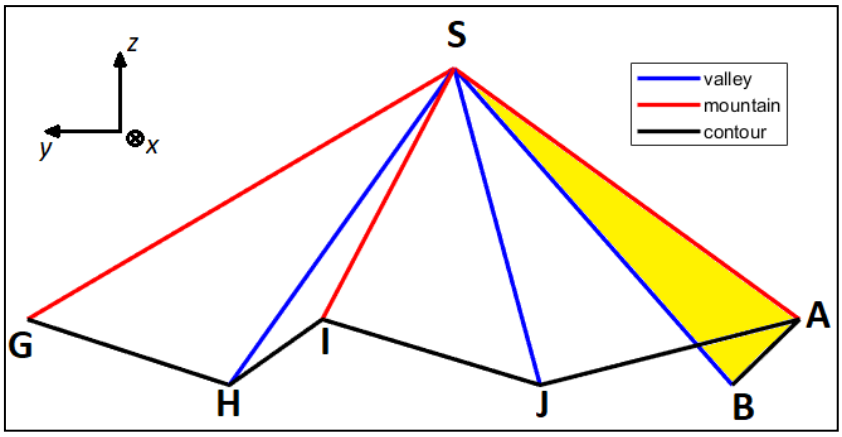

Figure 7. Schematic overview of the pentagonal model projected in yz-plane.

Using the same approach as for the triangular model the coordinates of the system can be expressed in these angles and the constants a, b and c. In order to constrain free motion in space point A is fixed in the origin, C is fixed in the y- and z-direction and G is fixed in the z-direction. Starting with A:

$$A = \begin{bmatrix} 0 \\ 0 \\ 0 \end{bmatrix}$$

B expressed with respect to A:

$$B = \begin{bmatrix} bcos(\theta)cos(\phi) \\ bsin(\theta)cos(\phi) \\ -bsin(\phi) \end{bmatrix}$$

C expressed with respect to B:

$$C = \begin{bmatrix} 2bcos(\theta)cos(\phi) \\ 0 \\ 0 \end{bmatrix}$$

And so forth until G:

$$D = \begin{bmatrix} C(1) + a * sin\left(-\theta + \frac{\pi}{10}\right) cos(\phi) \\ C(2) + a * cos\left(-\theta + \frac{\pi}{10}\right) cos(\phi) \\ C(3) - a * sin(\phi) \end{bmatrix}$$

$$E = \begin{bmatrix} D(1) + a * sin\left(\theta + \frac{\pi}{10}\right) cos(\phi) \\ D(2) + a * cos\left(\theta + \frac{\pi}{10}\right) cos(\phi) \\ D(3) + a * sin(\phi) \end{bmatrix}$$

$$F = \begin{bmatrix} E(1) - a * sin\left(\theta + \frac{3\pi}{10}\right) cos(\phi) \\ E(2) + a * cos\left(\theta + \frac{3\pi}{10}\right) cos(\phi) \\ E(3) - a * sin(\phi) \end{bmatrix}$$

$$G = \begin{bmatrix} F(1) - a * sin\left(-\theta + \frac{3\pi}{10}\right) cos(\phi) \\ F(2) + a * cos\left(-\theta + \frac{3\pi}{10}\right) cos(\phi) \\ F(3) + a * sin(\phi) \end{bmatrix}$$

The coordinates of J, I and H are expressed with respect to A:

$$J = \begin{bmatrix} -a * sin\left(-\theta + \frac{\pi}{10}\right) cos(\phi) \\ a * cos\left(-\theta + \frac{\pi}{10}\right) cos(\phi) \\ -a * sin(\phi) \end{bmatrix}$$

$$I = \begin{bmatrix} J(1) - a * sin\left(\theta + \frac{\pi}{10}\right) cos(\phi) \\ J(2) + a * cos\left(\theta + \frac{\pi}{10}\right) cos(\phi) \\ J(3) + a * sin(\phi) \end{bmatrix}$$

Lastly S is expressed with respect to B, due to symmetry they share the same x-coordinate:

$$S = \begin{bmatrix} B(1) \\ B(2) + b * sin(\psi) \\ B(3) + b * cos(\psi) \end{bmatrix}$$

The constraints are of the same type as the triangle model:

$$eq6: \quad d(S, C) - c = 0$$
$$eq7: \quad d(S, D) - b = 0$$
$$eq8: \quad d(S, E) - c = 0$$
$$eq9: \quad d(S.F) - b = 0$$

$$eq10: \quad d(S,G) - c = 0$$
$$eq11: \quad d(S,H) - b = 0$$
$$eq12: \quad d(S,I) - c = 0$$
$$eq13: \quad d(S,J) - b = 0$$

Nine different angles are used and there are eight constraints, meaning only one angle is needed as input for describing the system. Matlab is used to determine the other eight angles. With the coordinates coupled with the constraints it is possible to plot the system for different angles and thus determine the maximum contraction. The projected area in the xy-plane is determined by:

$$Area = (2bcos(\theta)\cos(\psi))^2 * \frac{5}{4}\sqrt{\frac{3+\sqrt{5}}{5-\sqrt{5}}}$$

For the initial state it follows:

$$\theta = 0, \psi = 0.0364\, rad, thus\ Area = 13.3609$$

For the end state it holds:

$$\theta = \frac{3\pi}{10} rad, \psi = 0.0176\, rad, thus\ Area = 4.6208$$

Yielding an area reduction of over 65 percent.

$$\frac{4.6208 - 13.3609}{13.3609} * 100\% = -65{,}4\%$$

In contrast to the 25 percent of the triangle, the better choice seems to be the pentagon as fundamental basis. For the whole Disdyakis Triacontahedron, there is need of twelve of these pentagons.

Appendix B: Degrees of Freedom

When the whole model will be built it is necessary to know how many degrees of freedom (DOF) it will have. This will be done with two ways: a multibody analysis approach and through linearization. The DoF's are counted in two ways to ensure correct answers.

Using the multibody dynamics approach the number of bodies and constraints are counted, see table 1. This methods shows that the triangle has 3 internal DoF's and the pentagon 7.

Table 1: Table determining the Degrees of Freedom (DoF) of both the triangular and pentagonal structure

	Body			Joint			Constraint	**Total**
	Number of bodies	DoF per body	**Total**	Number of revolute joints	DoF per revolute joint	**Total**	Number of over-constraints*	
Triangular structure	6	6	**36**	6	-5	**-30**	3	**9: 6 external 3 internal**
Pentagonal structure	10		**60**	10		**-50**	3	**13: 6 external 7 internal**

*The last hinges removes 5 DoF's: Translation in three directions and rotation in both lateral directions. However, the three translations were already fixed due to the structures forming a closed loop, creating three overconstraints.

To determine whether this is correct the DoF's of the triangle and the pentagon will be determined by constructing the Jacobian of all the constraints with respect to the xyz-coordinates of all the points. The size of the nullspace gives the number of DoF's. The details are given in the Matlab script, which is found in appendix D. This methods also yields 3 DoF's for the triangle and 7 for the pentagon.

With the knowledge that the pentagon has 7 DoF's, the DoF's of the whole structure can be determined, using the net of the DT. This can be done by visualizing the net of the DT as an mathematical graph. The nodes are the pentagons and the links represent the influence of one pentagon to the other. This methods assumes that each pentagon has 7 DoF's at most and that neighbouring pentagons can decrease this total since they are connected by an edge. This method yields that the full model will have 33 DoF's. This is illustrated in fig. 8. By constructing the Jacobian of the full model and determining the size of the nullspace, a value of 33 DoF's is also determined, this Matlab script is also found in appendix D.

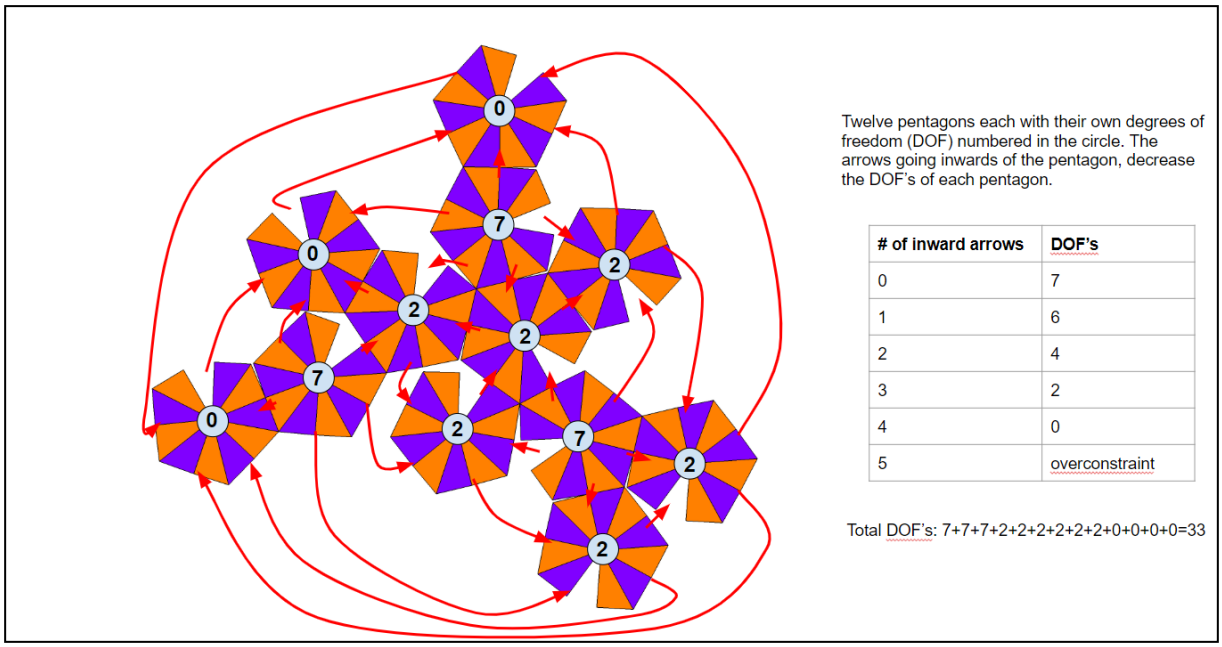

Figure 5. The net of the Disdyakis triacontahedron is depicted. For every single pentagon the degrees of freedom it possesses is shown in a white circle. With the red arrows it shows how the pentagons influence each other. The image is from Wikimedia.

Appendix C: Photo journal

C.1 SolidWorks Drawings

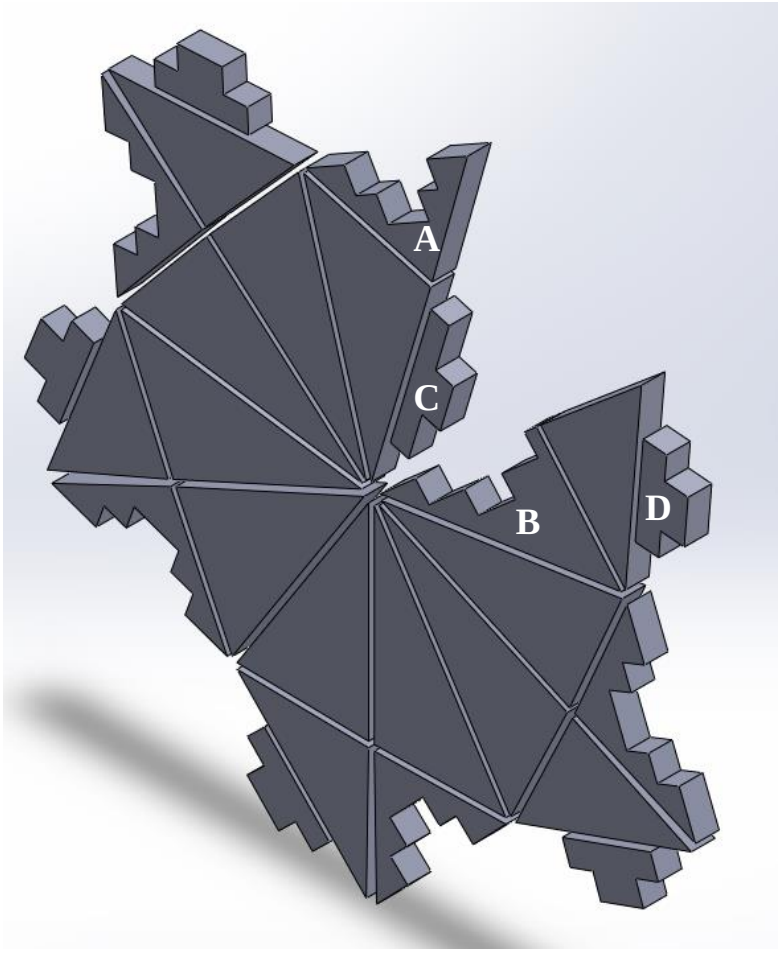

Figure 6. SolidWorks drawing of the pentagonal structure. The dimensions of parts A, B, C and D are given in the next figure.

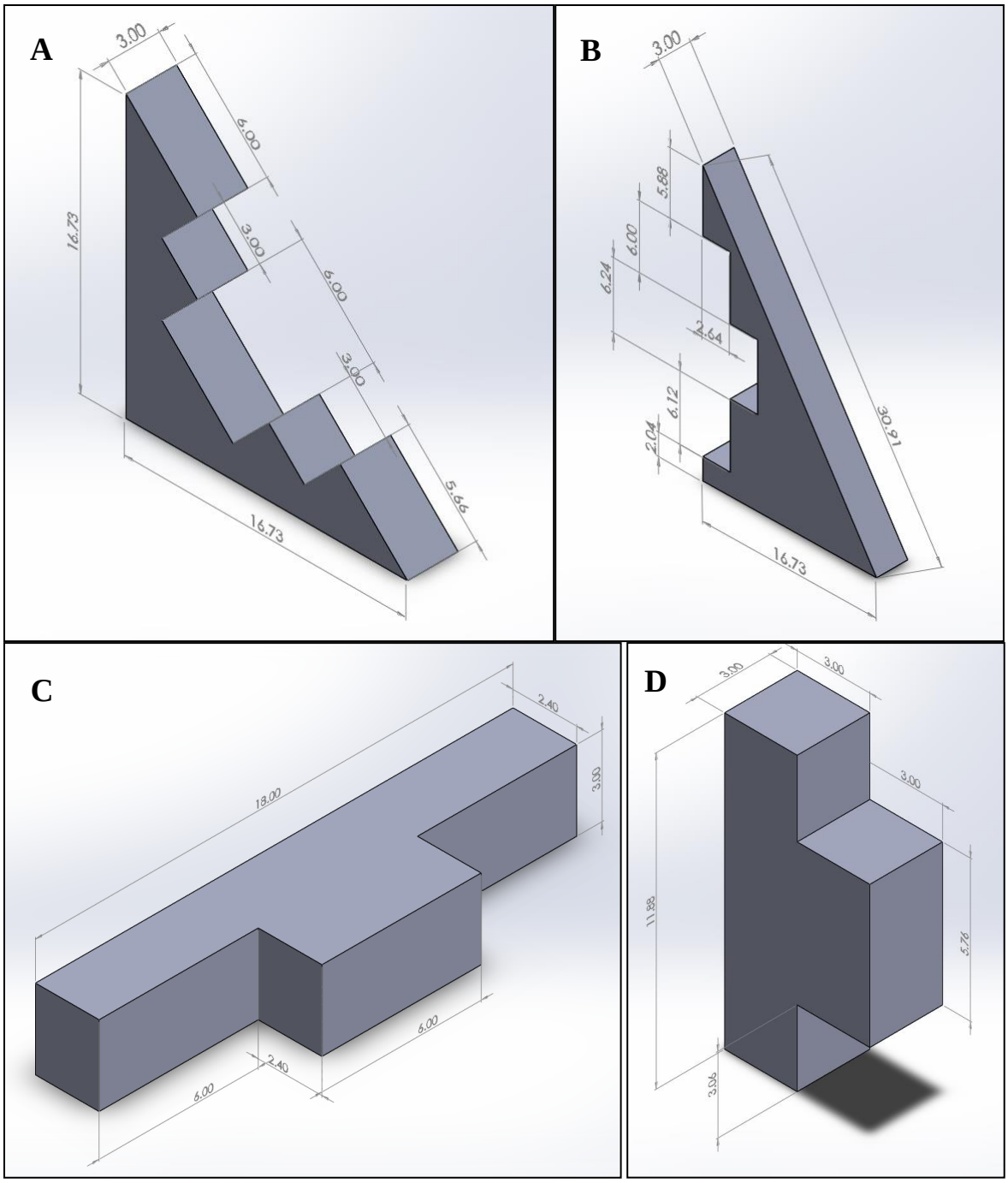

Figure 7. Zoomed in pictures of the SolidWorks drawing showing the dimensions of the parts.

C.2 Fabrication of the prototype

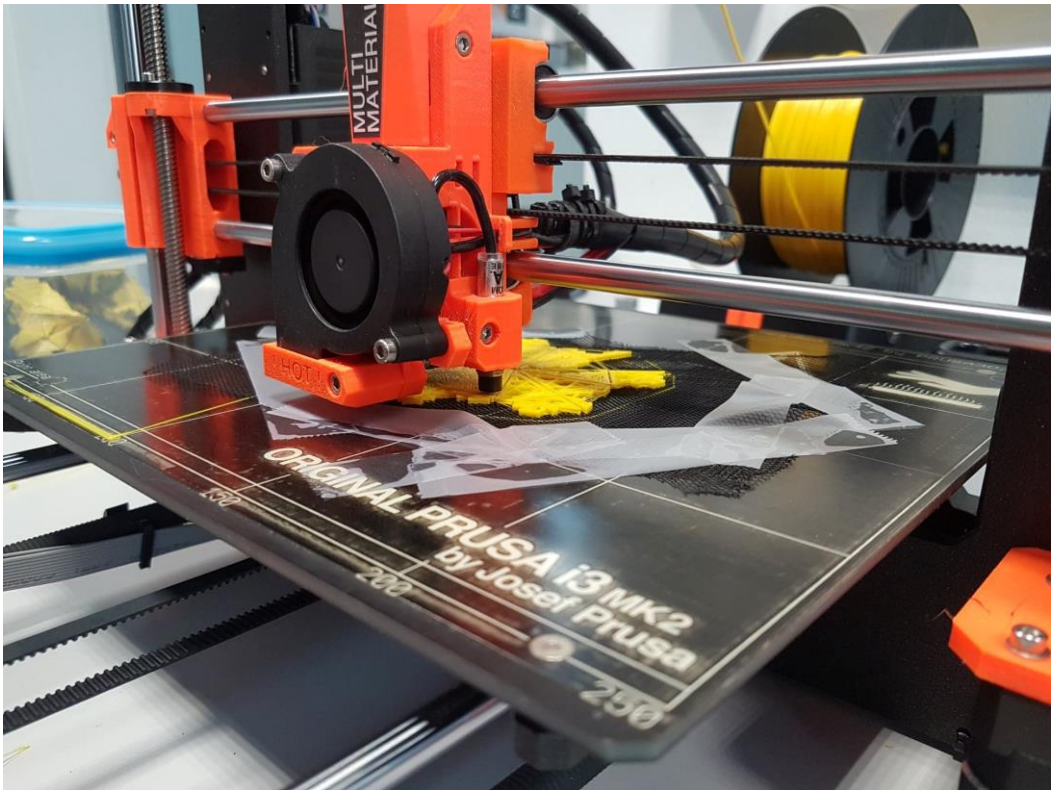

Figure 8. Photo showing the 3D-printing process. The netting is applied and kept positioned with tape.

Figure 9. Product after 3D-printing with the excessive netting cut away.

C.3 Photos of the prototype

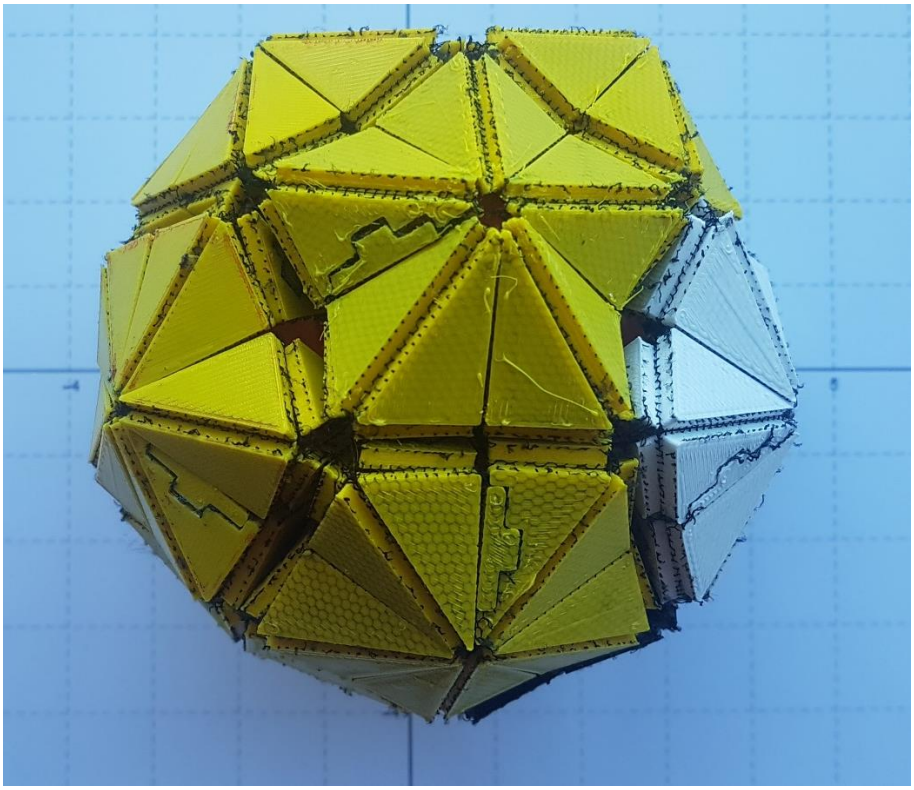

Figure 10. Photo of the prototype in initial state.

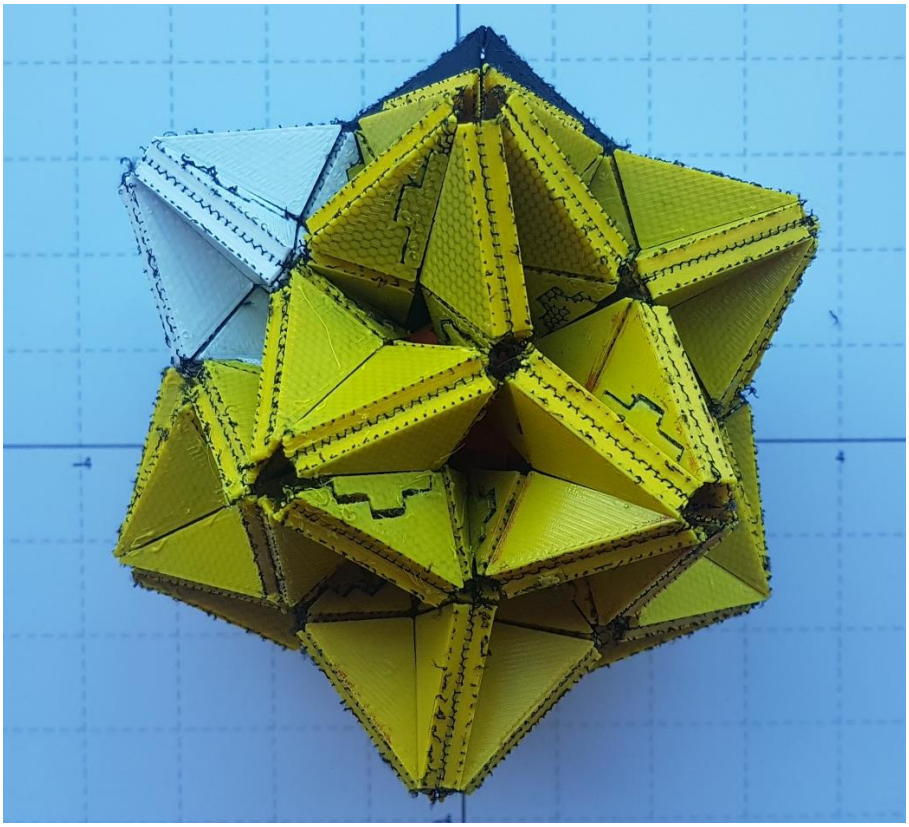

Figure 11. Photo of the prototype in final state

Appendix D: Matlab code

D.1 Script for the triangular structure

```
%Ivar Nuijts 10-1-2019
%triangle function thesis
close all
clc
clear all

%% Constants
a=sqrt(15*(85-31*sqrt(5)))/11;
b=3*sqrt(15*(65+19*sqrt(5)))/55;
c=2*sqrt(15*(5-sqrt(5)))/5;

%% Parameters
%input
theta=deg2rad(0);

syms phi psi

% %initial position
% theta=0;
% phi=pi/2-acos((a^2+3*b^2-c^2)/(2*sqrt(3)*a*b));
% psi=0;

% %final position
% theta=pi/6;
% phi=0;
% psi=0;

%% Coordinates
A=[0 0 0].'; %origin
B=[b*cos(psi)*cos(theta), b*sin(theta)*cos(psi), -b*sin(psi)].';
C=[2*b*cos(psi)*cos(theta), 0, 0].';
D=[2*b*cos(psi)*cos(theta)-b*sin(theta+pi/6)*cos(psi),
b*cos(psi)*cos(theta+pi/6), -b*sin(psi)].';
E=[D(1)-b*cos(theta+pi/3)*cos(psi),
b*cos(psi)*cos(theta+pi/6)+b*sin(theta+pi/3)*cos(psi), 0].';
F=[b*sin(theta+pi/6)*cos(psi), b*cos(theta+pi/6)*cos(psi), -
b*sin(psi)].';
S=[b*cos(psi)*cos(theta), b*sin(theta)*cos(psi)+a*sin(phi), -
b*sin(psi)+a*cos(phi)].';

%% Input theta, solving for phi en psi
%Applying two constraint equations. vector AS=c so constant as the first
%equation, the second equation is a cross section of the figure forming a
%triangle with sides a, c and BE

eq1=norm(S-E)-c==0;
eq2=norm(S-D)-a==0;

Solve= solve([eq1, eq2],[phi psi]);
psi=double(Solve.psi);
phi=double(Solve.phi);

%% plotting
X=[A(1), B(1), C(1), D(1), E(1), F(1), A(1)].';
Y=[A(2), B(2), C(2), D(2), E(2), F(2), A(2)].';
Z=[A(3), B(3), C(3), D(3), E(3), F(3), A(3)].';
Matrix=[A, S, B, S, C, S, D, S, E, S, F, S].';
X=double(subs(X, Solve));
```

```
Y=double(subs(Y, Solve));
Z=double(subs(Z, Solve));
A=double(subs(A, Solve));
B=double(subs(B, Solve));
C=double(subs(C, Solve));
D=double(subs(D, Solve));
E=double(subs(E, Solve));
F=double(subs(F, Solve));
S=double(subs(S, Solve));
Matrix=double(subs(Matrix, Solve));
figure
plot3(X, Y, Z, 'LineWidth', 1)
grid on
hold on
plot3(Matrix(:,1), Matrix(:,2), Matrix(:,3), 'LineWidth', 1)
axis equal
thetadeg=rad2deg(theta);
title(['\theta= ' num2str(thetadeg) ' deg'])
xlabel 'x'
ylabel 'y'
zlabel 'z'

%check is constraints are met
ABerror=(norm(A-B)-b);
ASerror=(norm(A-S)-c);
AFerror=(norm(A-F)-b);
BSerror=(norm(B-S)-a);
DSerror=(norm(D-S)-a);
FSerror=(norm(F-S)-a);
CSerror=(norm(C-S)-c);
ESerror=(norm(E-S)-c);

%% normal vectors
% lowerleft is 1, counting ccw
normal1=cross(A-B, A-S);
normal1=normal1/(norm(normal1));

normal2=cross(B-C, B-S);
normal2=normal2/(norm(normal2));

normal3=cross(C-D, C-S);
normal3=normal3/(norm(normal3));

normal4=cross(D-E, D-S);
normal4=normal4/(norm(normal4));

normal5=cross(E-F, E-S);
normal5=normal5/(norm(normal5));

normal6=cross(F-A, F-S);
normal6=normal6/(norm(normal6));

p1 = 180-atan2d(norm(cross(normal1,normal2)),dot(normal1,normal2));
p2 = 180-atan2d(norm(cross(normal2,normal3)),dot(normal2,normal3));

%% Check if symmetry assumption is valid.
%Assume different angles between C and E and check if different values
are
%possible. This only changes the coords of D
syms zeta delta epsilon
```

```
D2=[2*b*cos(psi)*cos(theta)-b*sin(zeta+pi/6)*cos(delta),
b*cos(delta)*cos(zeta+pi/6), -b*sin(psi)+a*cos(phi)-a*cos(epsilon)].';
S2=[b*cos(psi)*cos(theta), b*sin(theta)*cos(psi)+a*sin(phi), -
b*sin(psi)+a*cos(phi)].';

%zeta=theta
%delta=psi
%epsilon=phi

eq3=norm(D2-C)==b;
eq4=norm(D2-E)==b;
eq5=norm(D2-S2)==a;

Solve2=vpasolve([eq3 eq4 eq5], [zeta delta epsilon], [0 1; 0 1; 0 pi/2]);
zeta=double(Solve2.zeta);
delta=double(Solve2.delta);
epsilon=double(Solve2.epsilon);
%error
thetaError=(zeta-theta)*180/pi
psiError=(delta-psi)*180/pi
epsilonError=(epsilon-phi)*180/pi

%% plotting

D2=double(subs(D2, Solve2));
S2=double(subs(S2, Solve2));
X2=[A(1), B(1), C(1), D2(1), E(1), F(1), A(1)].';
Y2=[A(2), B(2), C(2), D2(2), E(2), F(2), A(2)].';
Z2=[A(3), B(3), C(3), D2(3), E(3), F(3), A(3)].';
Matrix2=[A, S2, B, S2, C, S2, D2, S2, E, S2, F, S2].';
figure
plot3(X2, Y2, Z2,'r', 'LineWidth', 0.5)
grid on
hold on
plot3(Matrix2(:,1), Matrix2(:,2), Matrix2(:,3),'r', 'LineWidth', 1)
plot3(X, Y, Z,'b', 'LineWidth', 1)
plot3(Matrix(:,1), Matrix(:,2), Matrix(:,3),'b', 'LineWidth', 1)
axis equal
```

D.2 Script for the pentagonal structure

```
% Ivar Nuijts
% Pentagon model

close all
clc
clear all

%% Constants
a=sqrt(15*(85-31*sqrt(5)))/11;
b=3*sqrt(15*(65+19*sqrt(5)))/55;
c=2*sqrt(15*(5-sqrt(5)))/5;
t1deg=45;
t1=deg2rad(t1deg);
syms p1 p2 p3 p4 k1 t2 t3 t4

%t in xy plane
%p in xz plane
%k in yz plane

%% coordinates
A=[ 0 0 0].'; %origin
B=[a*cos(t1)*cos(p1) a*sin(t1)*cos(p1) -a*sin(p1)].';
C=[B(1)+a*cos(t2)*cos(p2) B(2)-a*sin(t2)*cos(p2) B(3)+a*sin(p2)].';
D=[C(1)+a*sin(pi/10-t2)*cos(p2) C(2)+a*cos(pi/10-t2)*cos(p2) C(3)-
a*sin(p2)].';
E=[D(1)+a*sin(pi/10+t2)*cos(p3) D(2)+a*cos(pi/10+t2)*cos(p3)
D(3)+a*sin(p3)].';
F=[E(1)-a*sin(3*pi/10+t3)*cos(p3) E(2)+a*cos(3*pi/10+t3)*cos(p3) E(3)-
a*sin(p3)].';
G=[F(1)-a*sin(3*pi/10-t4)*cos(p4) F(2)+a*cos(3*pi/10-t4)*cos(p4)
F(3)+a*sin(p4)].';
J=[-a*sin(pi/10-t1)*cos(p1) a*cos(pi/10-t1)*cos(p1) -a*sin(p1)].';
I=[J(1)-a*sin(pi/10+t1)*cos(p1) J(2)+a*cos(pi/10+t1)*cos(p1)
J(3)+a*sin(p1)].';
H=[I(1)+a*sin(3*pi/10+t4)*cos(p1) I(2)+a*cos(3*pi/10+t4)*cos(p1) I(3)-
a*sin(p1)].';
S=[B(1) B(2)+b*sin(k1) B(3)+b*cos(k1)].';
%S=[B(1) B(2)+b*sin(k1) B(3)-b*cos(k1)].'; %flipping it upside down
%% constraint equations
eq1=norm(S-E)-c==0;
eq2=norm(S-C)-c==0;
eq3=norm(S-G)-c==0;
eq4=norm(S-I)-c==0;
eq5=norm(S-D)-b==0;
eq6=norm(S-F)-b==0;
eq7=norm(S-H)-b==0;
eq8=norm(S-J)-b==0;

Solve= solve([eq1, eq2, eq3, eq4, eq5, eq6, eq7, eq8],[p1 p2 p3 p4 k1 t2
t3 t4 ]);

p1=double(Solve.p1);
p2=double(Solve.p2);
p3=double(Solve.p3);
p4=double(Solve.p4);
k1=double(Solve.k1);
t2=double(Solve.t2);
t3=double(Solve.t3);
t4=double(Solve.t4);
%% plot
```

```
X=[A(1), B(1), C(1), D(1), E(1), F(1), G(1), H(1), I(1), J(1), A(1)].';
Y=[A(2), B(2), C(2), D(2), E(2), F(2), G(2), H(2), I(2), J(2), A(2)].';
Z=[A(3), B(3), C(3), D(3), E(3), F(3), G(3), H(3), I(3), J(3), A(3)].';
Matrix=[A, S, B, S, C, S, D, S, E, S, F, S, G, S, H, S, I, S, J].';

%subbing
X=double(subs(X, Solve));
Y=double(subs(Y, Solve));
Z=double(subs(Z, Solve));
A=double(subs(A, Solve));
B=double(subs(B, Solve));
C=double(subs(C, Solve));
D=double(subs(D, Solve));
E=double(subs(E, Solve));
F=double(subs(F, Solve));
G=double(subs(G, Solve));
H=double(subs(H, Solve));
I=double(subs(I, Solve));
J=double(subs(J, Solve));
S=double(subs(S, Solve));
Matrix=double(subs(Matrix, Solve));

figure
plot3(X, Y, Z,'b', 'LineWidth', 1)
grid on
hold on
plot3(Matrix(:,1), Matrix(:,2), Matrix(:,3),'b', 'LineWidth', 1)
axis equal

%% Area
Area=C(1)^2*1.25*sqrt((3+sqrt(5))/(5-sqrt(5)))
```

D.3 Script for plotting the full model

```
% Ivar Nuijts
% Disdyakis plot
close all
clc
clear all

%% Constants
a=sqrt(15*(85-31*sqrt(5)))/11;
b=3*sqrt(15*(65+19*sqrt(5)))/55;
c=2*sqrt(15*(5-sqrt(5)))/5;
t1deg=0;
t1=deg2rad(t1deg);

syms p1 p2 p3 p4 k1 t2 t3 t4

%t in xy plane
%p in xz plane
%k in yz plane

%% coordinates
A=[ 0 0 0].'; %origin
B=[a*cos(t1)*cos(p1) a*sin(t1)*cos(p1) -a*sin(p1)].';
C=[B(1)+a*cos(t2)*cos(p2) B(2)-a*sin(t2)*cos(p2) B(3)+a*sin(p2)].';
D=[C(1)+a*sin(pi/10-t2)*cos(p2) C(2)+a*cos(pi/10-t2)*cos(p2) C(3)-
a*sin(p2)].';
E=[D(1)+a*sin(pi/10+t2)*cos(p3) D(2)+a*cos(pi/10+t2)*cos(p3)
D(3)+a*sin(p3)].';
F=[E(1)-a*sin(3*pi/10+t3)*cos(p3) E(2)+a*cos(3*pi/10+t3)*cos(p3) E(3)-
a*sin(p3)].';
G=[F(1)-a*sin(3*pi/10-t4)*cos(p4) F(2)+a*cos(3*pi/10-t4)*cos(p4)
F(3)+a*sin(p4)].';
J=[-a*sin(pi/10-t1)*cos(p1) a*cos(pi/10-t1)*cos(p1) -a*sin(p1)].';
I=[J(1)-a*sin(pi/10+t1)*cos(p1) J(2)+a*cos(pi/10+t1)*cos(p1)
J(3)+a*sin(p1)].';
H=[I(1)+a*sin(3*pi/10+t4)*cos(p1) I(2)+a*cos(3*pi/10+t4)*cos(p1) I(3)-
a*sin(p1)].';
S=[B(1) B(2)+b*sin(k1) B(3)+b*cos(k1)].';
%S=[B(1) B(2)+b*sin(k1) B(3)-b*cos(k1)].'; %flipping inside out
%% constraint equations
eq1=norm(S-E)-c==0;
eq2=norm(S-C)-c==0;
eq3=norm(S-G)-c==0;
eq4=norm(S-I)-c==0;
eq5=norm(S-D)-b==0;
eq6=norm(S-F)-b==0;
eq7=norm(S-H)-b==0;
eq8=norm(S-J)-b==0;

Solve= solve([eq1, eq2, eq3, eq4, eq5, eq6, eq7, eq8],[p1 p2 p3 p4 k1 t2
t3 t4 ]);

p1=double(Solve.p1);
p2=double(Solve.p2);
p3=double(Solve.p3);
p4=double(Solve.p4);
k1=double(Solve.k1);
t2=double(Solve.t2);
t3=double(Solve.t3);
t4=double(Solve.t4);
%% plot
```

```
X=[A(1), B(1), C(1), D(1), E(1), F(1), G(1), H(1), I(1), J(1), A(1)].';
Y=[A(2), B(2), C(2), D(2), E(2), F(2), G(2), H(2), I(2), J(2), A(2)].';
Z=[A(3), B(3), C(3), D(3), E(3), F(3), G(3), H(3), I(3), J(3), A(3)].';
Matrix=[A, S, B, S, C, S, D, S, E, S, F, S, G, S, H, S, I, S, J].';

%subbing
X=double(subs(X, Solve));
Y=double(subs(Y, Solve));
Z=double(subs(Z, Solve));
A=double(subs(A, Solve));
B=double(subs(B, Solve));
C=double(subs(C, Solve));
D=double(subs(D, Solve));
E=double(subs(E, Solve));
F=double(subs(F, Solve));
G=double(subs(G, Solve));
H=double(subs(H, Solve));
I=double(subs(I, Solve));
J=double(subs(J, Solve));
S=double(subs(S, Solve));
Matrix=double(subs(Matrix, Solve));

figure
plot3(X, Y, Z,'b', 'LineWidth', 2)
hold on
plot3(Matrix(:,1), Matrix(:,2), Matrix(:,3),'b', 'LineWidth', 2)
axis equal

%plot second pentagon
di=acos(-1/sqrt(5));
di=rad2deg(di);
XYZ=[ X Y Z];
XYZ2=rotx(di)*XYZ';
Matrix2=rotx(di)*Matrix';
plot3(XYZ2(1,:), XYZ2(2,:), -XYZ2(3,:), 'r', 'LineWidth', 2)
plot3(Matrix2(1,:), Matrix2(2,:), -Matrix2(3,:),'r', 'LineWidth', 2)

%plot third pentagon
ra=deg2rad(-di);
u=I/norm(I);
%wikipedia
R=[ cos(ra)+u(1)*u(1)*(1-cos(ra)) u(1)*u(2)*(1-cos(ra))-u(3)*sin(ra)
u(1)*u(3)*(1-cos(ra))+u(2)*sin(ra);...
    u(2)*u(1)*(1-cos(ra))+u(3)*sin(ra) cos(ra)+u(2)*u(2)*(1-cos(ra))
u(2)*u(3)*(1-cos(ra))-u(1)*sin(ra);...
    u(3)*u(1)*(1-cos(ra))-u(2)*sin(ra) u(3)*u(2)*(1-cos(ra))+u(1)*sin(ra)
cos(ra)+u(3)*u(3)*(1-cos(ra))];
XYZ3=R*XYZ';
Matrix3=R*Matrix';
plot3(XYZ3(1,:), XYZ3(2,:), -XYZ3(3,:), 'g', 'LineWidth', 2)
plot3(Matrix3(1,:), Matrix3(2,:), -Matrix3(3,:),'g', 'LineWidth', 2)

%plot fourth pentagon
ra=deg2rad(180-di);
u=(E-C)/norm(E-C);
ras=4*pi/5;
%wikipedia
R=[ cos(ra)+u(1)*u(1)*(1-cos(ra)) u(1)*u(2)*(1-cos(ra))-u(3)*sin(ra)
u(1)*u(3)*(1-cos(ra))+u(2)*sin(ra);...
    u(2)*u(1)*(1-cos(ra))+u(3)*sin(ra) cos(ra)+u(2)*u(2)*(1-cos(ra))
u(2)*u(3)*(1-cos(ra))-u(1)*sin(ra);...
```

```
    u(3)*u(1)*(1-cos(ra))-u(2)*sin(ra) u(3)*u(2)*(1-cos(ra))+u(1)*sin(ra)
cos(ra)+u(3)*u(3)*(1-cos(ra))];

XYZ4=R*rotz(-36)*XYZ';
Matrix4=R*rotz(-36)*Matrix';
plot3(C(1)+XYZ4(1,:), XYZ4(2,:), XYZ4(3,:), 'y', 'LineWidth', 2)
plot3(C(1)+Matrix4(1,:), Matrix4(2,:), Matrix4(3,:),'y', 'LineWidth', 2)

%plot fifth pentagon
ra=deg2rad(180-di);
u=(G-E)/norm(G-E);
s=S/norm(S);
%wikipedia
R=[ cos(ra)+u(1)*u(1)*(1-cos(ra)) u(1)*u(2)*(1-cos(ra))-u(3)*sin(ra)
u(1)*u(3)*(1-cos(ra))+u(2)*sin(ra);...
    u(2)*u(1)*(1-cos(ra))+u(3)*sin(ra) cos(ra)+u(2)*u(2)*(1-cos(ra))
u(2)*u(3)*(1-cos(ra))-u(1)*sin(ra);...
    u(3)*u(1)*(1-cos(ra))-u(2)*sin(ra) u(3)*u(2)*(1-cos(ra))+u(1)*sin(ra)
cos(ra)+u(3)*u(3)*(1-cos(ra))];

XYZ5=R*rotz(54-18)*XYZ';
Matrix5=R*rotz(54-18)*Matrix';
plot3(E(1)+XYZ5(1,:),E(2)+XYZ5(2,:),E(3)+XYZ5(3,:), 'c', 'LineWidth', 2)
plot3(E(1)+Matrix5(1,:),E(2)+Matrix5(2,:),E(3)+Matrix5(3,:),'c',
'LineWidth', 2)

%plot sixth pentagon
ra=deg2rad(180-di);
u=(I-G)/norm(I-G);
R=[ cos(ra)+u(1)*u(1)*(1-cos(ra)) u(1)*u(2)*(1-cos(ra))-u(3)*sin(ra)
u(1)*u(3)*(1-cos(ra))+u(2)*sin(ra);...
    u(2)*u(1)*(1-cos(ra))+u(3)*sin(ra) cos(ra)+u(2)*u(2)*(1-cos(ra))
u(2)*u(3)*(1-cos(ra))-u(1)*sin(ra);...
    u(3)*u(1)*(1-cos(ra))-u(2)*sin(ra) u(3)*u(2)*(1-cos(ra))+u(1)*sin(ra)
cos(ra)+u(3)*u(3)*(1-cos(ra))];

XYZ6=R*rotz(90-54)*XYZ';
Matrix6=R*rotz(90-54)*Matrix';
plot3(I(1)+XYZ6(1,:),I(2)+XYZ6(2,:),I(3)+XYZ6(3,:), 'm', 'LineWidth', 2)
plot3(I(1)+Matrix6(1,:),I(2)+Matrix6(2,:),I(3)+Matrix6(3,:),'m',
'LineWidth', 2)

%plot seventh pentagon
%use the orientation of the third pentagon
ra=deg2rad(-di);
u=I/norm(I);
%wikipedia
R=[ cos(ra)+u(1)*u(1)*(1-cos(ra)) u(1)*u(2)*(1-cos(ra))-u(3)*sin(ra)
u(1)*u(3)*(1-cos(ra))+u(2)*sin(ra);...
    u(2)*u(1)*(1-cos(ra))+u(3)*sin(ra) cos(ra)+u(2)*u(2)*(1-cos(ra))
u(2)*u(3)*(1-cos(ra))-u(1)*sin(ra);...
    u(3)*u(1)*(1-cos(ra))-u(2)*sin(ra) u(3)*u(2)*(1-cos(ra))+u(1)*sin(ra)
cos(ra)+u(3)*u(3)*(1-cos(ra))];
XYZ7=XYZ';
Matrix7=Matrix';
XYZ7(3,:)=-XYZ7(3,:);
Matrix7(3,:)=-Matrix7(3,:);
XYZ7=R*rotz(144+180)*XYZ7;
Matrix7=R*rotz(144+180)*Matrix7;
plot3(C(1)+XYZ4(1,7)+XYZ7(1,:),XYZ4(2,7)+XYZ7(2,:),XYZ4(3,7)-XYZ7(3,:),
'g', 'LineWidth', 2)
```

```
plot3(C(1)+XYZ4(1,7)+Matrix7(1,:),XYZ4(2,7)+Matrix7(2,:),XYZ4(3,7)-
Matrix7(3,:),'g', 'LineWidth', 2)

%plot eight pentagon
%Take the orientation of the second pentagon
XYZ8=XYZ';
XYZ8(3,:)=-XYZ8(3,:);
XYZ8=rotx(di)*rotz(180+144)*XYZ8;
Matrix8=Matrix';
Matrix8(3,:)=-Matrix8(3,:);
Matrix8=rotx(di)*rotz(180+144)*Matrix8;
plot3(I(1)+XYZ6(1,7)+XYZ8(1,:),I(2)+XYZ6(2,7)+XYZ8(2,:),I(3)+XYZ6(3,7)-
XYZ8(3,:), 'r', 'LineWidth', 2)
plot3(I(1)+XYZ6(1,7)+Matrix8(1,:),I(2)+XYZ6(2,7)+Matrix8(2,:),I(3)+XYZ6(3
,7)-Matrix8(3,:),'r', 'LineWidth', 2)

%plot ninth pentagon
%use orientation of fourth pentagon
ra=deg2rad(180-di);
u=(E-C)/norm(E-C);
R=[ cos(ra)+u(1)*u(1)*(1-cos(ra)) u(1)*u(2)*(1-cos(ra))-u(3)*sin(ra)
u(1)*u(3)*(1-cos(ra))+u(2)*sin(ra);...
    u(2)*u(1)*(1-cos(ra))+u(3)*sin(ra) cos(ra)+u(2)*u(2)*(1-cos(ra))
u(2)*u(3)*(1-cos(ra))-u(1)*sin(ra);...
    u(3)*u(1)*(1-cos(ra))-u(2)*sin(ra) u(3)*u(2)*(1-cos(ra))+u(1)*sin(ra)
cos(ra)+u(3)*u(3)*(1-cos(ra))];
XYZ9=XYZ';
Matrix9=Matrix';
XYZ9(3,:)=-XYZ9(3,:);
Matrix9(3,:)=-Matrix9(3,:);
XYZ9=R*rotz(0)*XYZ9;
Matrix9=R*rotz(0)*Matrix9;
plot3(XYZ3(1,5)+XYZ9(1,:),XYZ3(2,5)+XYZ9(2,:),-XYZ3(3,5)+XYZ9(3,:), 'y',
'LineWidth', 2)
plot3(XYZ3(1,5)+Matrix9(1,:),XYZ3(2,5)+Matrix9(2,:),-
XYZ3(3,5)+Matrix9(3,:),'y', 'LineWidth', 2)

%plot tenth pentagon
ra=deg2rad(180-di);
u=(G-E)/norm(G-E);
R=[ cos(ra)+u(1)*u(1)*(1-cos(ra)) u(1)*u(2)*(1-cos(ra))-u(3)*sin(ra)
u(1)*u(3)*(1-cos(ra))+u(2)*sin(ra);...
    u(2)*u(1)*(1-cos(ra))+u(3)*sin(ra) cos(ra)+u(2)*u(2)*(1-cos(ra))
u(2)*u(3)*(1-cos(ra))-u(1)*sin(ra);...
    u(3)*u(1)*(1-cos(ra))-u(2)*sin(ra) u(3)*u(2)*(1-cos(ra))+u(1)*sin(ra)
cos(ra)+u(3)*u(3)*(1-cos(ra))];

XYZ10=XYZ';
Matrix10=Matrix';
XYZ10(3,:)=-XYZ10(3,:);
Matrix10(3,:)=-Matrix10(3,:);
XYZ10=R*rotz(0)*XYZ10;
Matrix10=R*rotz(0)*Matrix10;
plot3(XYZ3(1,3)+XYZ10(1,:),XYZ3(2,3)+XYZ10(2,:),-XYZ3(3,3)+XYZ10(3,:),
'c', 'LineWidth', 2)
plot3(XYZ3(1,3)+Matrix10(1,:),XYZ3(2,3)+Matrix10(2,:),-
XYZ3(3,3)+Matrix10(3,:),'c', 'LineWidth', 2)

%plot eleventh pentagon
ra=deg2rad(180-di);
u=(I-G)/norm(I-G);
```

```
R=[ cos(ra)+u(1)*u(1)*(1-cos(ra)) u(1)*u(2)*(1-cos(ra))-u(3)*sin(ra)
u(1)*u(3)*(1-cos(ra))+u(2)*sin(ra);...
    u(2)*u(1)*(1-cos(ra))+u(3)*sin(ra) cos(ra)+u(2)*u(2)*(1-cos(ra))
u(2)*u(3)*(1-cos(ra))-u(1)*sin(ra);...
    u(3)*u(1)*(1-cos(ra))-u(2)*sin(ra) u(3)*u(2)*(1-cos(ra))+u(1)*sin(ra)
cos(ra)+u(3)*u(3)*(1-cos(ra))];

XYZ11=XYZ';
Matrix11=Matrix';
XYZ11(3,:)=-XYZ11(3,:);
Matrix11(3,:)=-Matrix11(3,:);
XYZ11=R*rotz(0)*XYZ11;
Matrix11=R*rotz(0)*Matrix11;
plot3(XYZ2(1,7)+XYZ11(1,:),XYZ2(2,7)+XYZ11(2,:),-XYZ2(3,7)+XYZ11(3,:),
'm', 'LineWidth', 2)
plot3(XYZ2(1,7)+Matrix11(1,:),XYZ2(2,7)+Matrix11(2,:),-
XYZ2(3,7)+Matrix11(3,:),'m', 'LineWidth', 2)

%plot twelfth pentagon
XYZ12=XYZ';
Matrix12=Matrix';
XYZ12(3,:)=-XYZ12(3,:);
Matrix12(3,:)=-Matrix12(3,:);
XYZ12=rotz(36)*XYZ12;
Matrix12=rotz(36)*Matrix12;
plot3(XYZ3(1,3)+XYZ10(1,5)+XYZ12(1,:),XYZ3(2,3)+XYZ10(2,5)+XYZ12(2,:),-
XYZ3(3,3)+XYZ10(3,7)+XYZ12(3,:), 'b', 'LineWidth', 2)
plot3(XYZ3(1,3)+XYZ10(1,5)+Matrix12(1,:),XYZ3(2,3)+XYZ10(2,5)+Matrix12(2,
:),-XYZ3(3,3)+XYZ10(3,7)+Matrix12(3,:),'b', 'LineWidth', 2)
title(['Disdyakis Triacontahedron with angle=' num2str(54) ' deg'])
xlabel x
ylabel y
zlabel z
```

D.4 script for calculating Degrees of freedom triangular structure

```
% Ivar Nuijts
% Determining the DoF's of the triangle
close all
clear all
clc

%% Constants
a=sqrt(15*(85-31*sqrt(5)))/11;
b=3*sqrt(15*(65+19*sqrt(5)))/55;
c=2*sqrt(15*(5-sqrt(5)))/5;

%% variables
syms ax ay az bx by bz cx cy cz dx dy dz ex ey ez fx fy fz sx sy sz

V=[ax, ay, az, bx, by, bz, cx, cy, cz, dx, dy, dz, ex, ey, ez, fx, fy,
fz, sx, sy, sz].';

%% coordinates
A=[ax ay az].';
B=[bx by bz].';
C=[cx cy cz].';
D=[dx dy dz].';
E=[ex ey ez].';
F=[fx fy fz].';
S=[sx sy sz].';

%% constraints
%Point A is fixed in the origin
g1=ax;
g2=ay;
g3=az;
%Point C is fixed in y and z w.r.t A
g4=cy;
g5=cz;
%point E is fixed in z w.t.r. A
g6=ez;
%now the model is fixed in space

%constraint between points
%along the perimeter
g7=norm(B-A)-b;
g8=norm(C-B)-b;
g9=norm(D-C)-b;
g10=norm(E-D)-b;
g11=norm(F-E)-b;
g12=norm(A-F)-b;

%w.r.t the centre S
g13=norm(S-A)-c;
g14=norm(S-B)-a;
g15=norm(S-C)-c;
g16=norm(S-D)-a;
g17=norm(S-E)-c;
g18=norm(S-F)-a;

Q=[g1 g2 g3 g4 g5 g6 g7 g8 g9 g10 g11 g12 g13 g14 g15 g16 g17 g18].';

J=jacobian(Q,V);

%substitute for real coordinates.
```

```
theta=deg2rad(20); %initial state
syms psi phi
[ A, B, C, D, E, F, S ] = GetCoords( theta, phi, psi );

J=double((subs(J,[ax ay az bx by bz cx cy cz dx dy dz ex ey ez fx fy fz
sx sy sz].',[ A; B; C; D; E; F; S ])));
N=null(J);
DOF=size(N,2)

%coordinates initial state
X=[A(1), B(1), C(1), D(1), E(1), F(1), A(1)].';
Y=[A(2), B(2), C(2), D(2), E(2), F(2), A(2)].';
Z=[A(3), B(3), C(3), D(3), E(3), F(3), A(3)].';
Matrix=[A, S, B, S, C, S, D, S, E, S, F, S].';

for i=1:DOF
Anew=A+0.5*N(1:3,i);
Bnew=B+0.5*N(4:6,i);
Cnew=C+0.5*N(7:9,i);
Dnew=D+0.5*N(10:12,i);
Enew=E+0.5*N(13:15,i);
Fnew=F+0.5*N(16:18,i);
Snew=S+0.5*N(19:21,i);

Xnew=[Anew(1), Bnew(1), Cnew(1), Dnew(1), Enew(1), Fnew(1), Anew(1)].';
Ynew=[Anew(2), Bnew(2), Cnew(2), Dnew(2), Enew(2), Fnew(2), Anew(2)].';
Znew=[Anew(3), Bnew(3), Cnew(3), Dnew(3), Enew(3), Fnew(3), Anew(3)].';
Matrixnew=[Anew, Snew, Bnew, Snew, Cnew, Snew, Dnew, Snew, Enew, Snew,
Fnew, Snew].';

subplot(1,3,i)
p1=plot3(X, Y, Z,'b', 'LineWidth', 1)
grid on
hold on
plot3(Matrix(:,1), Matrix(:,2), Matrix(:,3),'b', 'LineWidth', 1)
axis equal
p2=plot3(Xnew, Ynew, Znew,'r', 'LineWidth', 1)
plot3(Matrixnew(:,1), Matrixnew(:,2), Matrixnew(:,3),'r', 'LineWidth', 1)
title(['state' num2str(i)])
view(2)
end
legend([p1 p2],{'Initial state', 'Linearized next state'})
```

```
function [ A, B, C, D, E, F, S ] = GetCoords( theta, phi, psi )
%Coordinates based on the angles theta, phi and psi
% the input is theta, psi and phi are calculated. Need to be syms first.
%% constants
a=sqrt(15*(85-31*sqrt(5)))/11;
b=3*sqrt(15*(65+19*sqrt(5)))/55;
c=2*sqrt(15*(5-sqrt(5)))/5;

%% coordinates
A=[0 0 0].'; %origin
B=[b*cos(psi)*cos(theta), b*sin(theta)*cos(psi), -b*sin(psi)].';
C=[2*b*cos(psi)*cos(theta), 0, 0].';
D=[2*b*cos(psi)*cos(theta)-b*sin(theta+pi/6)*cos(psi),
b*cos(psi)*cos(theta+pi/6), -b*sin(psi)].';
E=[D(1)-b*cos(theta+pi/3)*cos(psi),
b*cos(psi)*cos(theta+pi/6)+b*sin(theta+pi/3)*cos(psi), 0].';
F=[b*sin(theta+pi/6)*cos(psi), b*cos(theta+pi/6)*cos(psi), -
b*sin(psi)].';
```

```
S=[b*cos(psi)*cos(theta), b*sin(theta)*cos(psi)+a*sin(phi), -
b*sin(psi)+a*cos(phi)].';
%% Input theta, solving for phi en psi
%Applying two constraint equations. vector AS=c so constant as the first
%equation, the second equation is a cross section of the figure forming a
%triangle with sides a, c and BE

eq1=norm(S-E)-c==0;
eq2=norm(S-D)-a==0;

Solve= solve([eq1, eq2],[phi psi]);
psi=Solve.psi;
phi=Solve.phi;

%% Coordinates subbed
A=double(subs(A, Solve));
B=double(subs(B, Solve));
C=double(subs(C, Solve));
D=double(subs(D, Solve));
E=double(subs(E, Solve));
F=double(subs(F, Solve));
S=double(subs(S, Solve));

%PlotCoords=[A B C D E F A S B S C S D S E S F];
end
```

D.5 script for calculating Degrees of freedom pentagonal structure

```
% Ivar Nuijts
% Determining the DoF's of the pentagon
close all
clear all
clc

%% Constants
a=sqrt(15*(85-31*sqrt(5)))/11;
b=3*sqrt(15*(65+19*sqrt(5)))/55;
c=2*sqrt(15*(5-sqrt(5)))/5;

%% variables
syms ax ay az bx by bz cx cy cz dx dy dz ex ey ez fx fy fz gx gy gz hx hy
hz ix iy iz jx jy jz sx sy sz

V=[ax ay az bx by bz cx cy cz dx dy dz ex ey ez fx fy fz gx gy gz hx hy
hz ix iy iz jx jy jz sx sy sz];

%% coordinates
A=[ax ay az].';
B=[bx by bz].';
C=[cx cy cz].';
D=[dx dy dz].';
E=[ex ey ez].';
F=[fx fy fz].';
G=[gx gy gz].';
H=[hx hy hz].';
I=[ix iy iz].';
J=[jx jy jz].';
S=[sx sy sz].';

%% constraints
%Point A is fixed in the origin
g1=ax;
g2=ay;
g3=az;
%Point C is fixed in y and z w.r.t A
g4=cy;
g5=cz;
%point G is fixed in z w.t.r. A
g6=gz;
%now the model is fixed in space

%constraint between points
%along the perimeter
g7=norm(A-B)-a;
g8=norm(C-B)-a;
g9=norm(D-C)-a;
g10=norm(E-D)-a;
g11=norm(F-E)-a;
g12=norm(G-F)-a;
g13=norm(H-G)-a;
g14=norm(I-H)-a;
g15=norm(J-I)-a;
g16=norm(A-J)-a;
%w.r.t the centre S
g17=norm(S-A)-c;
g18=norm(S-B)-c;
g19=norm(S-C)-c;
g20=norm(S-D)-c;
```

```
g21=norm(S-E)-c;
g22=norm(S-F)-c;
g23=norm(S-G)-c;
g24=norm(S-H)-c;
g25=norm(S-I)-c;
g26=norm(S-J)-c;

Q=[ g1 g2 g3 g4 g5 g6 g7 g8 g9 g10 g11 g12 g13 g14 g15 g16 g17 g18 g19
g20 g21 g22 g23 g24 g25 g26].';

Jac=jacobian(Q,V);

t1=deg2rad(25);
syms p1 p2 p3 p4 k1 t2 t3 t4

[ A, B, C, D, E, F, G, H, I, J, S ] = GetPentaCoords(t1, t2, t3, t4, p1,
p2, p3, p4, k1);

Jac=double((subs(Jac,[ax ay az bx by bz cx cy cz dx dy dz ex ey ez fx fy
fz gx gy gz hx hy hz ix iy iz jx jy jz sx sy sz].',[ A; B; C; D; E; F; G;
H; I; J; S ])));
N=null(Jac);
DOF=size(N,2)

%coordinates initial state
X=[A(1), B(1), C(1), D(1), E(1), F(1), G(1), H(1), I(1), J(1), A(1)].';
Y=[A(2), B(2), C(2), D(2), E(2), F(2), G(2), H(2), I(2), J(2), A(2)].';
Z=[A(3), B(3), C(3), D(3), E(3), F(3), G(3), H(3), I(3), J(3), A(3)].';
Matrix=[A, S, B, S, C, S, D, S, E, S, F, S, G, S, H, S, I, S, J].';

for i=1:DOF
Anew=A+0.5*N(1:3,i);
Bnew=B+0.5*N(4:6,i);
Cnew=C+0.5*N(7:9,i);
Dnew=D+0.5*N(10:12,i);
Enew=E+0.5*N(13:15,i);
Fnew=F+0.5*N(16:18,i);
Gnew=G+0.5*N(19:21,i);
Hnew=H+0.5*N(22:24,i);
Inew=I+0.5*N(25:27,i);
Jnew=J+0.5*N(28:30,i);
Snew=S+0.5*N(31:33,i);

Xnew=[Anew(1), Bnew(1), Cnew(1), Dnew(1), Enew(1), Fnew(1), Gnew(1),
Hnew(1), Inew(1), Jnew(1), Anew(1)].';
Ynew=[Anew(2), Bnew(2), Cnew(2), Dnew(2), Enew(2), Fnew(2), Gnew(2),
Hnew(2), Inew(2), Jnew(2), Anew(2)].';
Znew=[Anew(3), Bnew(3), Cnew(3), Dnew(3), Enew(3), Fnew(3), Gnew(3),
Hnew(3), Inew(3), Jnew(3), Anew(3)].';
Matrixnew=[Anew, Snew, Bnew, Snew, Cnew, Snew, Dnew, Snew, Enew, Snew,
Fnew, Snew, Gnew, Snew, Hnew, Snew, Inew, Snew, Jnew, Snew, Jnew].';

subplot(2,4,i)
p1=plot3(X, Y, Z,'b', 'LineWidth', 1);
grid on
hold on
plot3(Matrix(:,1), Matrix(:,2), Matrix(:,3),'b', 'LineWidth', 1)
axis equal
p2=plot3(Xnew, Ynew, Znew,'r', 'LineWidth', 1);
plot3(Matrixnew(:,1), Matrixnew(:,2), Matrixnew(:,3),'r', 'LineWidth', 1)
title(['state' num2str(i)])
```

```
view(2)
end
legend([p1 p2],{'Initial state', 'Linearized next state'})
```

```
function [ A, B, C, D, E, F, G, H, I, J, S ] = GetPentaCoords( t1, t2,
t3, t4, p1, p2, p3, p4, k1)
% Ivar Nuijts
% Pentagon model
%% Constants
a=sqrt(15*(85-31*sqrt(5)))/11;
b=3*sqrt(15*(65+19*sqrt(5)))/55;
c=2*sqrt(15*(5-sqrt(5)))/5;

% p1=deg2rad(0);
% p2=deg2rad(0);
% p3=deg2rad(0);
% p4=deg2rad(0);
% k1=pi/3; %not correct yet

%t in xy plane
%p in xz plane
%k in yz plane

%% coordinates
A=[ 0 0 0].'; %origin
B=[a*cos(t1)*cos(p1) a*sin(t1)*cos(p1) -a*sin(p1)].';
C=[B(1)+a*cos(t2)*cos(p2) B(2)-a*sin(t2)*cos(p2) B(3)+a*sin(p2)].';
D=[C(1)+a*sin(pi/10-t2)*cos(p2) C(2)+a*cos(pi/10-t2)*cos(p2) C(3)-
a*sin(p2)].';
E=[D(1)+a*sin(pi/10+t2)*cos(p3) D(2)+a*cos(pi/10+t2)*cos(p3)
D(3)+a*sin(p3)].';
F=[E(1)-a*sin(3*pi/10+t3)*cos(p3) E(2)+a*cos(3*pi/10+t3)*cos(p3) E(3)-
a*sin(p3)].';
G=[F(1)-a*sin(3*pi/10-t4)*cos(p4) F(2)+a*cos(3*pi/10-t4)*cos(p4)
F(3)+a*sin(p4)].';
J=[-a*sin(pi/10-t1)*cos(p1) a*cos(pi/10-t1)*cos(p1) -a*sin(p1)].';
I=[J(1)-a*sin(pi/10+t1)*cos(p1) J(2)+a*cos(pi/10+t1)*cos(p1)
J(3)+a*sin(p1)].';
H=[I(1)+a*sin(3*pi/10+t4)*cos(p1) I(2)+a*cos(3*pi/10+t4)*cos(p1) I(3)-
a*sin(p1)].';
S=[B(1) B(2)+b*sin(k1) B(3)+b*cos(k1)].';

%% constraint equations
eq1=norm(S-E)-c==0;
eq2=norm(S-C)-c==0;
eq3=norm(S-G)-c==0;
eq4=norm(S-I)-c==0;
eq5=norm(S-D)-b==0;
eq6=norm(S-F)-b==0;
eq7=norm(S-H)-b==0;
eq8=norm(S-J)-b==0;

Solve= solve([eq1, eq2, eq3, eq4, eq5, eq6, eq7, eq8],[p1 p2 p3 p4 k1 t2
t3 t4 ]);

%% subbing
A=double(subs(A, Solve));
B=double(subs(B, Solve));
C=double(subs(C, Solve));
D=double(subs(D, Solve));
```

```
E=double(subs(E, Solve));
F=double(subs(F, Solve));
G=double(subs(G, Solve));
H=double(subs(H, Solve));
I=double(subs(I, Solve));
J=double(subs(J, Solve));
S=double(subs(S, Solve));

end
```

D.6 script for calculating Degrees of freedom full model

```
%Ivar Nuijts
%Disdyakis DOFs
close all
clear all
clc
%values from:
%http://dmccooey.com/polyhedra/DisdyakisTriacontahedron.txt

%% Constants
C0 = 1.17518645301134929748244365923;
C1 = 1.38196601125010515179541316563;
C2 = 1.90149162409079437985955492738 53;
C3 = 2.17082039324993690892275210062;
C4 = 2.23606797749978969640917366873;
C5 = 3.07667807710214367734199293309;
C6 = 3.51246117974981072676825630186;
C7 = 3.61803398874989484820458683437;
C8 = 3.80298324818158875971909854771;

a=sqrt(15*(85-31*sqrt(5)))/11;
b=3*sqrt(15*(65+19*sqrt(5)))/55;
c=2*sqrt(15*(5-sqrt(5)))/5;
%the following points will be split:
% 0 1 2 3 4 5 30 31 32 33 34 35 36 37 38 39 40 41 42 43 44 45 46 47 48 49
% 50 51 52 53
%% variables
syms V0X V0Y V0Z V1X V1Y V1Z V2X V2Y V2Z V3X V3Y V3Z V4X V4Y V4Z V5X V5Y
V5Z V6X V6Y V6Z V7X V7Y V7Z V8X V8Y V8Z V9X V9Y V9Z ...
    V10X V10Y V10Z V11X V11Y V11Z V12X V12Y V12Z V13X V13Y V13Z V14X V14Y
V14Z V15X V15Y V15Z V16X V16Y V16Z V17X V17Y V17Z V18X V18Y V18Z V19X
V19Y V19Z ...
    V20X V20Y V20Z V21X V21Y V21Z V22X V22Y V22Z V23X V23Y V23Z V24X V24Y
V24Z V25X V25Y V25Z V26X V26Y V26Z V27X V27Y V27Z V28X V28Y V28Z V29X
V29Y V29Z ...
    V30X V30Y V30Z V31X V31Y V31Z V32X V32Y V32Z V33X V33Y V33Z V34X V34Y
V34Z V35X V35Y V35Z V36X V36Y V36Z V37X V37Y V37Z V38X V38Y V38Z V39X
V39Y V39Z ...
    V40X V40Y V40Z V41X V41Y V41Z V42X V42Y V42Z V43X V43Y V43Z V44X V44Y
V44Z V45X V45Y V45Z V46X V46Y V46Z V47X V47Y V47Z V48X V48Y V48Z V49X
V49Y V49Z ...
    V50X V50Y V50Z V51X V51Y V51Z V52X V52Y V52Z V53X V53Y V53Z V54X V54Y
V54Z V55X V55Y V55Z V56X V56Y V56Z V57X V57Y V57Z V58X V58Y V58Z V59X
V59Y V59Z ...
    V60X V60Y V60Z V61X V61Y V61Z

syms V0XB V0YB V0ZB V1XB V1YB V1ZB V2XB V2YB V2ZB V3XB V3YB V3ZB V4XB
V4YB V4ZB V5XB V5YB V5ZB V30XB V30YB V30ZB V31XB V31YB V31ZB V32XB V32YB
V32ZB V33XB V33YB V33ZB V34XB V34YB V34ZB...
     V35XB V35YB V35ZB V36XB V36YB V36ZB V37XB V37YB V37ZB V38XB V38YB
V38ZB V39XB V39YB V39ZB V40XB V40YB V40ZB V41XB V41YB V41ZB V42XB V42YB
V42ZB V43XB V43YB V43ZB V44XB V44YB ...
     V44ZB V45XB V45YB V45ZB V46XB V46YB V46ZB V47XB V47YB V47ZB V48XB
V48YB V48ZB V49XB V49YB V49ZB V50XB V50YB V50ZB V51XB V51YB V51ZB V52XB
V52YB V52ZB V53XB V53YB V53ZB

Vec=[V0X V0Y V0Z V1X V1Y V1Z V2X V2Y V2Z V3X V3Y V3Z V4X V4Y V4Z V5X V5Y
V5Z V6X V6Y V6Z V7X V7Y V7Z V8X V8Y V8Z V9X V9Y V9Z ...
    V10X V10Y V10Z V11X V11Y V11Z V12X V12Y V12Z V13X V13Y V13Z V14X V14Y
V14Z V15X V15Y V15Z V16X V16Y V16Z V17X V17Y V17Z V18X V18Y V18Z V19X
V19Y V19Z ...
```

```
    V20X V20Y V20Z V21X V21Y V21Z V22X V22Y V22Z V23X V23Y V23Z V24X V24Y
V24Z V25X V25Y V25Z V26X V26Y V26Z V27X V27Y V27Z V28X V28Y V28Z V29X
V29Y V29Z ...
    V30X V30Y V30Z V31X V31Y V31Z V32X V32Y V32Z V33X V33Y V33Z V34X V34Y
V34Z V35X V35Y V35Z V36X V36Y V36Z V37X V37Y V37Z V38X V38Y V38Z V39X
V39Y V39Z ...
    V40X V40Y V40Z V41X V41Y V41Z V42X V42Y V42Z V43X V43Y V43Z V44X V44Y
V44Z V45X V45Y V45Z V46X V46Y V46Z V47X V47Y V47Z V48X V48Y V48Z V49X
V49Y V49Z ...
    V50X V50Y V50Z V51X V51Y V51Z V52X V52Y V52Z V53X V53Y V53Z V54X V54Y
V54Z V55X V55Y V55Z V56X V56Y V56Z V57X V57Y V57Z V58X V58Y V58Z V59X
V59Y V59Z ...
    V60X V60Y V60Z V61X V61Y V61Z V0XB V0YB V0ZB V1XB V1YB V1ZB V2XB V2YB
V2ZB V3XB V3YB V3ZB V4XB V4YB V4ZB V5XB V5YB V5ZB V30XB V30YB V30ZB V31XB
V31YB V31ZB V32XB V32YB V32ZB V33XB V33YB V33ZB V34XB V34YB V34ZB...
     V35XB V35YB V35ZB V36XB V36YB V36ZB V37XB V37YB V37ZB V38XB V38YB
V38ZB V39XB V39YB V39ZB V40XB V40YB V40ZB V41XB V41YB V41ZB V42XB V42YB
V42ZB V43XB V43YB V43ZB V44XB V44YB ...
     V44ZB V45XB V45YB V45ZB V46XB V46YB V46ZB V47XB V47YB V47ZB V48XB
V48YB V48ZB V49XB V49YB V49ZB V50XB V50YB V50ZB V51XB V51YB V51ZB V52XB
V52YB V52ZB V53XB V53YB V53ZB].';
%% Coordinates
V0  =  [V0X V0Y V0Z].';
V1  =  [V1X V1Y V1Z].';
V2  =  [V2X V2Y V2Z].';
V3  =  [V3X V3Y V3Z].';
V4  =  [V4X V4Y V4Z].';
V5  =  [V5X V5Y V5Z].';
V0B  = [V0XB V0YB V0ZB].';
V1B  = [V1XB V1YB V1ZB].';
V2B  = [V2XB V2YB V2ZB].';
V3B  = [V3XB V3YB V3ZB].';
V4B  = [V4XB V4YB V4ZB].';
V5B  = [V5XB V5YB V5ZB].';
V6  =  [V6X V6Y V6Z].';
V7  =  [V7X V7Y V7Z].';
V8  =  [V8X V8Y V8Z].';
V9  =  [V9X V9Y V9Z].';
V10  = [V10X V10Y V10Z].';
V11  = [V11X V11Y V11Z].';
V12  = [V12X V12Y V12Z].';
V13  = [V13X V13Y V13Z].';
V14  = [V14X V14Y V14Z].';
V15  = [V15X V15Y V15Z].';
V16  = [V16X V16Y V16Z].';
V17  = [V17X V17Y V17Z].';
V18  = [V18X V18Y V18Z].';
V19  = [V19X V19Y V19Z].';
V20  = [V20X V20Y V20Z].';
V21  = [V21X V21Y V21Z].';
V22  = [V22X V22Y V22Z].';
V23  = [V23X V23Y V23Z].';
V24  = [V24X V24Y V24Z].';
V25  = [V25X V25Y V25Z].';
V26  = [V26X V26Y V26Z].';
V27  = [V27X V27Y V27Z].';
V28  = [V28X V28Y V28Z].';
V29  = [V29X V29Y V29Z].';
V30  = [V30X V30Y V30Z].';
V31  = [V31X V31Y V31Z].';
V32  = [V32X V32Y V32Z].';
```

```
V33  = [V33X V33Y V33Z].';
V34  = [V34X V34Y V34Z].';
V35  = [V35X V35Y V35Z].';
V36  = [V36X V36Y V36Z].';
V37  = [V37X V37Y V37Z].';
V38  = [V38X V38Y V38Z].';
V39  = [V39X V39Y V39Z].';
V40  = [V40X V40Y V40Z].';
V41  = [V41X V41Y V41Z].';
V42  = [V42X V42Y V42Z].';
V43  = [V43X V43Y V43Z].';
V44  = [V44X V44Y V44Z].';
V45  = [V45X V45Y V45Z].';
V46  = [V46X V46Y V46Z].';
V47  = [V47X V47Y V47Z].';
V48  = [V48X V48Y V48Z].';
V49  = [V49X V49Y V49Z].';
V50  = [V50X V50Y V50Z].';
V51  = [V51X V51Y V51Z].';
V52  = [V52X V52Y V52Z].';
V53  = [V53X V53Y V53Z].';
V30B  = [V30XB V30YB V30ZB].';
V31B  = [V31XB V31YB V31ZB].';
V32B  = [V32XB V32YB V32ZB].';
V33B  = [V33XB V33YB V33ZB].';
V34B  = [V34XB V34YB V34ZB].';
V35B  = [V35XB V35YB V35ZB].';
V36B  = [V36XB V36YB V36ZB].';
V37B  = [V37XB V37YB V37ZB].';
V38B  = [V38XB V38YB V38ZB].';
V39B  = [V39XB V39YB V39ZB].';
V40B  = [V40XB V40YB V40ZB].';
V41B  = [V41XB V41YB V41ZB].';
V42B  = [V42XB V42YB V42ZB].';
V43B  = [V43XB V43YB V43ZB].';
V44B  = [V44XB V44YB V44ZB].';
V45B  = [V45XB V45YB V45ZB].';
V46B  = [V46XB V46YB V46ZB].';
V47B  = [V47XB V47YB V47ZB].';
V48B  = [V48XB V48YB V48ZB].';
V49B  = [V49XB V49YB V49ZB].';
V50B  = [V50XB V50YB V50ZB].';
V51B  = [V51XB V51YB V51ZB].';
V52B  = [V52XB V52YB V52ZB].';
V53B  = [V53XB V53YB V53ZB].';
V54  = [V54X V54Y V54Z].';
V55  = [V55X V55Y V55Z].';
V56  = [V56X V56Y V56Z].';
V57  = [V57X V57Y V57Z].';
V58  = [V58X V58Y V58Z].';
V59  = [V59X V59Y V59Z].';
V60  = [V60X V60Y V60Z].';
V61  = [V61X V61Y V61Z].';

%% constraints
% fixing in space by fixing V0 V8 V18. V8  = [0.0, -C1,  C7]'; V18 = [
C3, 0.0,  C6]';
g1=V0X;
g2=V0Y;
g3=V0Z-C8;
g4=V8X;
```

```
g5=V8Y+C1;
g6=V8Z-C8;
g7=V18X-C3;
g8=V18Y;
g9=V18Z-C6;
%from point 18
g10=norm(V18-V0)-b;
g11=norm(V18-V8)-c;
g12=norm(V18-V32)-b;
g13=norm(V18-V56)-c;
g14=norm(V18-V40)-b;
g15=norm(V18-V10)-c;
g16=norm(V18-V38)-b;
g17=norm(V18-V54)-c;
g18=norm(V18-V30)-b;
g19=norm(V18-V6)-c;
%from poin 19
g20=norm(V19-V1)-b;
g21=norm(V19-V7)-c;
g22=norm(V19-V31)-b;
g23=norm(V19-V55)-c;
g24=norm(V19-V39)-b;
g25=norm(V19-V11)-c;
g26=norm(V19-V41)-b;
g27=norm(V19-V57)-c;
g28=norm(V19-V33)-b;
g29=norm(V19-V9)-c;
%from poin 20
g30=norm(V20-V0B)-b;
g31=norm(V20-V6)-c;
g32=norm(V20-V34)-b;
g33=norm(V20-V58)-c;
g34=norm(V20-V42)-b;
g35=norm(V20-V12)-c;
g36=norm(V20-V44)-b;
g37=norm(V20-V60)-c;
g38=norm(V20-V36)-b;
g39=norm(V20-V8)-c;
%from point 21
g40=norm(V21-V1B)-b;
g41=norm(V21-V9)-c;
g42=norm(V21-V37)-b;
g43=norm(V21-V61)-c;
g44=norm(V21-V45)-b;
g45=norm(V21-V13)-c;
g46=norm(V21-V43)-b;
g47=norm(V21-V59)-c;
g48=norm(V21-V35)-b;
g49=norm(V21-V7)-c;
%from point 22
g50=norm(V22-V2)-b;
g51=norm(V22-V11)-c;
g52=norm(V22-V39B)-b;
g53=norm(V22-V55)-c;
g54=norm(V22-V47)-b;
g55=norm(V22-V14)-c;
g56=norm(V22-V46)-b;
g57=norm(V22-V54)-c;
g58=norm(V22-V38B)-b;
g59=norm(V22-V10)-c;
%from point 23
```

```
g60=norm(V23-V2B)-b;
g61=norm(V23-V10)-c;
g62=norm(V23-V40B)-b;
g63=norm(V23-V56)-c;
g64=norm(V23-V48)-b;
g65=norm(V23-V15)-c;
g66=norm(V23-V49)-b;
g67=norm(V23-V57)-c;
g68=norm(V23-V41B)-b;
g69=norm(V23-V11)-c;
%from point 24
g70=norm(V24-V3)-b;
g71=norm(V24-V12)-c;
g72=norm(V24-V42B)-b;
g73=norm(V24-V58)-c;
g74=norm(V24-V50)-b;
g75=norm(V24-V16)-c;
g76=norm(V24-V51)-b;
g77=norm(V24-V59)-c;
g78=norm(V24-V43B)-b;
g79=norm(V24-V13)-c;
%from point 25
g80=norm(V25-V3B)-b;
g81=norm(V25-V13)-c;
g82=norm(V25-V45B)-b;
g83=norm(V25-V61)-c;
g84=norm(V25-V53)-b;
g85=norm(V25-V17)-c;
g86=norm(V25-V52)-b;
g87=norm(V25-V60)-c;
g88=norm(V25-V44B)-b;
g89=norm(V25-V12)-c;
%from point 26
g90=norm(V26-V4)-b;
g91=norm(V26-V16)-c;
g92=norm(V26-V50B)-b;
g93=norm(V26-V58)-c;
g94=norm(V26-V34B)-b;
g95=norm(V26-V6)-c;
g96=norm(V26-V30B)-b;
g97=norm(V26-V54)-c;
g98=norm(V26-V46B)-b;
g99=norm(V26-V14)-c;
%from point 27
g100=norm(V27-V4B)-b;
g101=norm(V27-V14)-c;
g102=norm(V27-V47B)-b;
g103=norm(V27-V55)-c;
g104=norm(V27-V31B)-b;
g105=norm(V27-V7)-c;
g106=norm(V27-V35B)-b;
g107=norm(V27-V59)-c;
g108=norm(V27-V51B)-b;
g109=norm(V27-V16)-c;
%from point 28
g110=norm(V28-V5)-b;
g111=norm(V28-V15)-c;
g112=norm(V28-V48B)-b;
g113=norm(V28-V56)-c;
g114=norm(V28-V32B)-b;
g115=norm(V28-V8)-c;
```

```
g116=norm(V28-V36B)-b;
g117=norm(V28-V60)-c;
g118=norm(V28-V52B)-b;
g119=norm(V28-V17)-c;
%from point 29
g120=norm(V29-V5B)-b;
g121=norm(V29-V17)-c;
g122=norm(V29-V53B)-b;
g123=norm(V29-V61)-c;
g124=norm(V29-V37B)-b;
g125=norm(V29-V9)-c;
g126=norm(V29-V33B)-b;
g127=norm(V29-V57)-c;
g128=norm(V29-V49B)-b;
g129=norm(V29-V15)-c;

%around point 18
g130=norm(V0-V8)-a;
g131=norm(V8-V32)-a;
g132=norm(V32-V56)-a;
g133=norm(V56-V40)-a;
g134=norm(V40-V10)-a;
g135=norm(V10-V38)-a;
g136=norm(V38-V54)-a;
g137=norm(V54-V30)-a;
g138=norm(V30-V6)-a;
g139=norm(V6-V1)-a;
%Extra constraints when the points split
g130B=norm(V0B-V8)-a;
g131B=norm(V8-V32B)-a;
g132B=norm(V32B-V56)-a;
g133B=norm(V56-V40B)-a;
g134B=norm(V40B-V10)-a;
g135B=norm(V10-V38B)-a;
g136B=norm(V38B-V54)-a;
g137B=norm(V54-V30B)-a;
g138B=norm(V30B-V6)-a;
g139B=norm(V6-V1B)-a;

%around point 19
g140=norm(V1-V7)-a;
g141=norm(V7-V31)-a;
g142=norm(V31-V55)-a;
g143=norm(V55-V39)-a;
g144=norm(V39-V11)-a;
g145=norm(V11-V41)-a;
g146=norm(V41-V57)-a;
g147=norm(V57-V33)-a;
g148=norm(V33-V9)-a;
g149=norm(V9-V1)-a;
%Extra constraints when the points split
g140B=norm(V1B-V7)-a;
g141B=norm(V7-V31B)-a;
g142B=norm(V31B-V55)-a;
g143B=norm(V55-V39B)-a;
g144B=norm(V39B-V11)-a;
g145B=norm(V11-V41B)-a;
g146B=norm(V41B-V57)-a;
g147B=norm(V57-V33B)-a;
g148B=norm(V33B-V9)-a;
g149B=norm(V9-V1B)-a;
```

```
%around point 20 2 overconstraints
g150=norm(V6-V34)-a;
g151=norm(V34-V58)-a;
g152=norm(V58-V42)-a;
g153=norm(V42-V12)-a;
g154=norm(V12-V44)-a;
g155=norm(V44-V60)-a;
g156=norm(V60-V36)-a;
g157=norm(V36-V8)-a;
%Extra constraints when the points split
g150B=norm(V6-V34B)-a;
g151B=norm(V34B-V58)-a;
g152B=norm(V58-V42B)-a;
g153B=norm(V42B-V12)-a;
g154B=norm(V12-V44B)-a;
g155B=norm(V44B-V60)-a;
g156B=norm(V60-V36B)-a;
g157B=norm(V36B-V8)-a;

%around point 21 2 overconstraints
g158=norm(V9-V37)-a;
g159=norm(V37-V61)-a;
g160=norm(V61-V45)-a;
g161=norm(V45-V13)-a;
g162=norm(V13-V43)-a;
g163=norm(V43-V59)-a;
g164=norm(V59-V35)-a;
g165=norm(V35-V7)-a;
%Extra constraints when the points split
g158B=norm(V9-V37B)-a;
g159B=norm(V37B-V61)-a;
g160B=norm(V61-V45B)-a;
g161B=norm(V45B-V13)-a;
g162B=norm(V13-V43B)-a;
g163B=norm(V43B-V59)-a;
g164B=norm(V59-V35B)-a;
g165B=norm(V35B-V7)-a;

%around point 22 4 overconstraints
g166=norm(V2-V11)-a;
g167=norm(V55-V47)-a;
g168=norm(V47-V14)-a;
g169=norm(V14-V46)-a;
g170=norm(V46-V54)-a;
g171=norm(V10-V2)-a;
%Extra constraints when the points split
g166B=norm(V2B-V11)-a;
g167B=norm(V55-V47B)-a;
g168B=norm(V47B-V14)-a;
g169B=norm(V14-V46B)-a;
g170B=norm(V46B-V54)-a;
g171B=norm(V10-V2B)-a;

%around point 23 6 overconstraints
g172=norm(V56-V48)-a;
g173=norm(V48-V15)-a;
g174=norm(V15-V49)-a;
g175=norm(V49-V57)-a;
%Extra constraints when the points split
g172B=norm(V56-V48B)-a;
```

```
g173B=norm(V48B-V15)-a;
g174B=norm(V15-V49B)-a;
g175B=norm(V49B-V57)-a;

%around point 24 4 overconstraints
g176=norm(V3-V12)-a;
g177=norm(V58-V50)-a;
g178=norm(V50-V16)-a;
g179=norm(V16-V51)-a;
g180=norm(V51-V59)-a;
g181=norm(V13-V3)-a;
%Extra constraints when the points split
g176B=norm(V3B-V12)-a;
g177B=norm(V58-V50B)-a;
g178B=norm(V50B-V16)-a;
g179B=norm(V16-V51B)-a;
g180B=norm(V51B-V59)-a;
g181B=norm(V13-V3B)-a;

%around point 25 6 overconstraints
g182=norm(V61-V53)-a;
g183=norm(V53-V17)-a;
g184=norm(V17-V52)-a;
g185=norm(V52-V60)-a;
%Extra constraints when the points split
g182B=norm(V61-V53B)-a;
g183B=norm(V53B-V17)-a;
g184B=norm(V17-V52B)-a;
g185B=norm(V52B-V60)-a;

%around point 26 8 overconstraints
g186=norm(V4-V16)-a;
g187=norm(V14-V4)-a;
%Extra constraints when the points split
g186B=norm(V4B-V16)-a;
g187B=norm(V14-V4B)-a;

%around point 27 10 overconstraints

%around point 28 8 overconstraints
g188=norm(V4-V16)-a;
g189=norm(V17-V5)-a;
%Extra constraints when the points split
g188B=norm(V4B-V16)-a;
g189B=norm(V17-V5B)-a;

%around point 29 10 overconstraints

Q=[ g1 g2 g3 g4 g5 g6 g7 g8 g9 g10 g11 g12 g13 g14 g15 g16 g17 g18 g19
g20 g21 g22 g23 g24 g25 g26 g27 g28 g29 g30 g31 g32 g33 g34 g35...
    g36 g37 g38 g39 g40 g41 g42 g43 g44 g45 g46 g47 g48 g49 g50 g51 g52
g53 g54 g55 g56 g57 g58 g59 g60 g61 g62 g63 g64 g65 g66 g67 g68...
    g69 g70 g71 g72 g73 g74 g75 g76 g77 g78 g79 g80 g81 g82 g83 g84 g85
g86 g87 g88 g89 g90 g91 g92 g93 g94 g95 g96 g97 g98 g99 g100 g101...
    g102 g103 g104 g105 g106 g107 g108 g109 g110 g111 g112 g113 g114 g115
g116 g117 g118 g119 g120 g121 g122 g123 g124 g125 g126 g127 g128...
    g129 g130 g131 g132 g133 g134 g135 g136 g137 g138 g139 g140 g141 g142
g143 g144 g145 g146 g147 g148 g149 g150 g151 g152 g153 g154 g155...
    g156 g157 g158 g159 g160 g161 g162 g163 g164 g165 g166 g167 g168 g169
g170 g171 g172 g173 g174 g175 g176 g177 g178 g179 g180 g181 g182...
```

```
    g183 g184 g185 g186 g187 g188 g189 g130B g131B g132B g133B g134B
g135B g136B g137B g138B g139B g140B g141B g142B g143B g144B g145B
g146B...
    g147B g148B g149B g150B g151B g152B g153B g154B g155B g156B g157B
g158B g159B g160B g161B g162B g163B g164B g165B g166B g167B g168B
g169B...
    g170B g171B g172B g173B g174B g175B g176B g177B g178B g179B g180B
g181B g182B g183B g184B g185B g186B g187B g188B g189B].';

Jac=jacobian(Q,Vec);

%% Points
V0  = [0.0 0.0  C8]';
V1  = [0.0 0.0 -C8]';
V2  = [ C8, 0.0, 0.0]';
V3  = [-C8, 0.0, 0.0]';
V4  = [0.0,  C8, 0.0]';
V5  = [0.0, -C8, 0.0]';
V6  = [0.0,  C1,  C7]';
V7  = [0.0,  C1, -C7]';
V8  = [0.0, -C1,  C7]';
V9  = [0.0, -C1, -C7]';
V10 = [ C7, 0.0,  C1]';
V11 = [ C7, 0.0, -C1]';
V12 = [-C7, 0.0,  C1]';
V13 = [-C7, 0.0, -C1]';
V14 = [ C1,  C7, 0.0]';
V15 = [ C1, -C7, 0.0]';
V16 = [-C1,  C7, 0.0]';
V17 = [-C1, -C7, 0.0]';
V18 = [ C3, 0.0,  C6]';
V19 = [ C3, 0.0, -C6]';
V20 = [-C3, 0.0,  C6]';
V21 = [-C3, 0.0, -C6]';
V22 = [ C6,  C3, 0.0]';
V23 = [ C6, -C3, 0.0]';
V24 = [-C6,  C3, 0.0]';
V25 = [-C6, -C3, 0.0]';
V26 = [0.0,  C6,  C3]';
V27 = [0.0,  C6, -C3]';
V28 = [0.0, -C6,  C3]';
V29 = [0.0, -C6, -C3]';
V30 = [ C0,  C2,  C5]';
V31 = [ C0,  C2, -C5]';
V32 = [ C0, -C2,  C5]';
V33 = [ C0, -C2, -C5]';
V34 = [-C0,  C2,  C5]';
V35 = [-C0,  C2, -C5]';
V36 = [-C0, -C2,  C5]';
V37 = [-C0, -C2, -C5]';
V38 = [ C5,  C0,  C2]';
V39 = [ C5,  C0, -C2]';
V40 = [ C5, -C0,  C2]';
V41 = [ C5, -C0, -C2]';
V42 = [-C5,  C0,  C2]';
V43 = [-C5,  C0, -C2]';
V44 = [-C5, -C0,  C2]';
V45 = [-C5, -C0, -C2]';
V46 = [ C2,  C5,  C0]';
V47 = [ C2,  C5, -C0]';
V48 = [ C2, -C5,  C0]';
```

```
V49 = [ C2, -C5, -C0]';
V50 = [-C2,  C5,  C0]';
V51 = [-C2,  C5, -C0]';
V52 = [-C2, -C5,  C0]';
V53 = [-C2, -C5, -C0]';
V54 = [ C4,  C4,  C4]';
V55 = [ C4,  C4, -C4]';
V56 = [ C4, -C4,  C4]';
V57 = [ C4, -C4, -C4]';
V58 = [-C4,  C4,  C4]';
V59 = [-C4,  C4, -C4]';
V60 = [-C4, -C4,  C4]';
V61 = [-C4, -C4, -C4]';

V0B  = [0.0 0.0  C8]';
V1B  = [0.0 0.0 -C8]';
V2B  = [ C8, 0.0, 0.0]';
V3B  = [-C8, 0.0, 0.0]';
V4B  = [0.0,  C8, 0.0]';
V5B  = [0.0, -C8, 0.0]';
V30B = [ C0,  C2,  C5]';
V31B = [ C0,  C2, -C5]';
V32B = [ C0, -C2,  C5]';
V33B = [ C0, -C2, -C5]';
V34B = [-C0,  C2,  C5]';
V35B = [-C0,  C2, -C5]';
V36B = [-C0, -C2,  C5]';
V37B = [-C0, -C2, -C5]';
V38B = [ C5,  C0,  C2]';
V39B = [ C5,  C0, -C2]';
V40B = [ C5, -C0,  C2]';
V41B = [ C5, -C0, -C2]';
V42B = [-C5,  C0,  C2]';
V43B = [-C5,  C0, -C2]';
V44B = [-C5, -C0,  C2]';
V45B = [-C5, -C0, -C2]';
V46B = [ C2,  C5,  C0]';
V47B = [ C2,  C5, -C0]';
V48B = [ C2, -C5,  C0]';
V49B = [ C2, -C5, -C0]';
V50B = [-C2,  C5,  C0]';
V51B = [-C2,  C5, -C0]';
V52B = [-C2, -C5,  C0]';
V53B = [-C2, -C5, -C0]';

Jac=double((subs(Jac,[V0X V0Y V0Z V1X V1Y V1Z V2X V2Y V2Z V3X V3Y V3Z V4X
V4Y V4Z V5X V5Y V5Z V6X V6Y V6Z V7X V7Y V7Z V8X V8Y V8Z V9X V9Y V9Z ...
    V10X V10Y V10Z V11X V11Y V11Z V12X V12Y V12Z V13X V13Y V13Z V14X V14Y
V14Z V15X V15Y V15Z V16X V16Y V16Z V17X V17Y V17Z V18X V18Y V18Z V19X
V19Y V19Z ...
    V20X V20Y V20Z V21X V21Y V21Z V22X V22Y V22Z V23X V23Y V23Z V24X V24Y
V24Z V25X V25Y V25Z V26X V26Y V26Z V27X V27Y V27Z V28X V28Y V28Z V29X
V29Y V29Z ...
    V30X V30Y V30Z V31X V31Y V31Z V32X V32Y V32Z V33X V33Y V33Z V34X V34Y
V34Z V35X V35Y V35Z V36X V36Y V36Z V37X V37Y V37Z V38X V38Y V38Z V39X
V39Y V39Z ...
    V40X V40Y V40Z V41X V41Y V41Z V42X V42Y V42Z V43X V43Y V43Z V44X V44Y
V44Z V45X V45Y V45Z V46X V46Y V46Z V47X V47Y V47Z V48X V48Y V48Z V49X
V49Y V49Z ...
```

```
    V50X V50Y V50Z V51X V51Y V51Z V52X V52Y V52Z V53X V53Y V53Z V54X V54Y
V54Z V55X V55Y V55Z V56X V56Y V56Z V57X V57Y V57Z V58X V58Y V58Z V59X
V59Y V59Z ...
    V60X V60Y V60Z V61X V61Y V61Z V0XB V0YB V0ZB V1XB V1YB V1ZB V2XB V2YB
V2ZB V3XB V3YB V3ZB V4XB V4YB V4ZB V5XB V5YB V5ZB V30XB V30YB V30ZB V31XB
V31YB V31ZB V32XB V32YB V32ZB V33XB V33YB V33ZB V34XB V34YB V34ZB...
     V35XB V35YB V35ZB V36XB V36YB V36ZB V37XB V37YB V37ZB V38XB V38YB
V38ZB V39XB V39YB V39ZB V40XB V40YB V40ZB V41XB V41YB V41ZB V42XB V42YB
V42ZB V43XB V43YB V43ZB V44XB V44YB ...
     V44ZB V45XB V45YB V45ZB V46XB V46YB V46ZB V47XB V47YB V47ZB V48XB
V48YB V48ZB V49XB V49YB V49ZB V50XB V50YB V50ZB V51XB V51YB V51ZB V52XB
V52YB V52ZB V53XB V53YB V53ZB].',[ V0; V1; V2; V3; V4; V5; V6; V7; V8;
V9; V10; V11; V12; V13; V14; V15; V16; V17; V18; V19;...
    V20; V21; V22; V23; V24; V25; V26; V27; V28; V29; V30; V31; V32; V33;
V34; V35; V36; V37; V38; V39; V40; V41; V42; V43; V44; V45; ...
    V46; V47; V48; V49; V50; V51; V52; V53; V54; V55; V56; V57; V58; V59;
V60; V61; V0B; V1B; V2B; V3B; V4B; V5B; V30B; V31B; V32B; V33B; V34B;
V35B; V36B; V37B; V38B; V39B; V40B; V41B; V42B; V43B; V44B; V45B; ...
    V46B; V47B; V48B; V49B; V50B; V51B; V52B; V53B])));
N=null(Jac);
DOF=size(N,2)
```